Symmetry-selective resonant inelastic x-ray scattering of C_{60}

Yi Luo, Hans Ågren, and Faris Gel'mukhanov
Institute of Physics and Measurement Technology, Linköping University, S-58183, Linköping, Sweden

Jinghua Guo, Per Skytt, Nial Wassdahl, and Joseph Nordgren
Department of Physics, Uppsala University, Box 530, S-75121 Uppsala, Sweden
(Received 25 August 1994; revised manuscript received 5 June 1995)

The resonantly excited x-ray emission spectra of the C_{60} molecule are presented and analyzed in terms of symmetry- and polarization-selective resonant inelastic scattering processes (RIXS). The theoretical analysis implements recently derived formalisms for symmetry-selective x-ray scattering. Isolated properties of the RIXS spectra are simulated and their cooperative action for the buildup of various features in RIXS of C_{60} are analyzed. Apart from symmetry and polarization dependences, the role of Stokes shifts, tail excitation, vibrational excitation, and interference effects are simulated in detail. Other relevant aspects are discussed in a more brief manner, such as influence of vibronic coupling and nonresonant anomalous contributions. Several conclusions about the nature of RIXS from C_{60} have been derived. The symmetry- and parity-selective character of the RIXS spectra is clearly visualized by excitation in the band gap. The symmetry selectivity leads to a strong correlation between the shape of the RIXS spectrum and the shape of the spectral function describing the incoming excitation photons. It also implies that the RIXS spectra become sparse in the limits of long core hole state lifetime and narrow-band excitation. Spectra pertaining to higher resonant energies involving a higher density of core-excited states are less symmetry selective and turn progressively into their broadband excitation and nonresonant analogues. Tail excitation and Stokes shifts have strong influence on the appearance of the RIXS spectra, both depending crucially on frequency and form of the spectral functions of the incoming photons and on the vibrational progressions of the core-excited states. The band-gap generated spectra emerge as consequences of Stokes shifts when the absorption energies are detuned from the lowest unoccupied molecular orbital resonance. The polarization and angular dependences of RIXS in C_{60} are found to be comparatively weak, something which is rationalized by the highly degenerate electronic structure and the spherical shape of the molecule. The computer simulations in this work rest on transition moments and energies obtained by *ab initio* Hartree-Fock calculations in the full I_h point-group symmetry.

I. INTRODUCTION

Perhaps no other single molecular species has been the subject to such a world-wide intense research effort as the fullerene molecule C_{60}. The proposal of the existence of the fullerene and the discovery of methods for producing it in macroscopic quantities initiated a great number of experimental and theoretical studies of its electronic and geometric properties. Out of many experimental methods employed, the family of core electron spectroscopies have found particularly fruitful applications, as exemplified by photoelectrons,[1,2] electron-energy-loss,[3,4] x-ray absorption,[5,6,4,7] Auger,[8] and x-ray emission[9] spectroscopies. The development of tunable narrow-band synchrotron radiation sources with high brightness has stimulated studies of the resonant counterparts of these techniques, i.e., resonant Auger (autoionization) and x-ray emission spectroscopies, synonymous with resonant nonradiative and radiative Raman spectroscopy, respectively. The interest in these resonant spectroscopies derives from the potentially rich, but yet very much unexplored, information they provide about electronic structure and scattering dynamics.

The achievements in resonant x-ray Raman-scattering spectroscopy originate in the use of monochromatic x-ray excitation with small spectral widths, sometimes smaller than the lifetime broadening of the core-excited states, and from the ability to continuously tune incoming x-ray frequencies near the ionization threshold. Using these techniques the sensitive dependence of the x-ray fluorescence on the frequency and spectral shape of the exciting radiation has been established. Resonance narrowing below the lifetime width leads to superhigh resolution and to linear dispersions of the resonant inelastic x-ray scattering (RIXS); the width of an x-ray emission line is defined only by the small lifetime broadening of the final optically excited state, and by the spectral width of the incoming radiation. The possibility to use linearly or circularly polarized radiation gives the opportunity to unequivocally assign all resolved electronic states for molecules of any symmetry, as recently shown in Ref. 10. Contemporary spectral equipment with high-intensity and narrow-bandpass x-ray photon sources produces RIXS spectra very rich of structures.

The analysis of RIXS requires in general a one-step theoretical formalism. The traditional two-step formulation, which assumes the x-ray emission to be decoupled

0163-1829/95/52(20)/14479(18)/$06.00

from the x-ray-absorption process, has applicability in the nonresonant case far from threshold, but only in special cases for near-threshold excitation in the region where resonant processes operate. Interpretation of nonresonant x-ray emission as a one-step process was proposed in the 1970s, by Gel'mukhanov and co-workers,[11–14] who introduced the notion of x-ray *channel interference,* and applied this to investigations of x-ray scattering in solids[13] and molecules,[12] and to vibronic fine-structure analysis of x-ray spectra. This effect, which is not encompassed by conventional two-step theory, takes place when the intermediate core-excited states are coherently excited. The x-ray scattering channels defined by these different core-excited states will interfere when the energy gaps are of the same order of magnitude as the lifetime broadening. Such interference is mostly relevant for resonant x-ray spectra in the elastic mode, the polarization and angular distributions of H_2S being a recently studied example,[15] but also takes place among vibronic channels in RIXS spectra. More recent formulations of x-ray processes are based on one-step many-channel resonant and off-resonant scattering theory, as introduced by Åberg and co-workers.[16–19]

The one-step formulations of RIXS lead to a Kramers-Heisenberg-type dispersion formula for the cross section, with generally only the resonant part of the scattering process taken into account. Using this starting point RIXS has been analyzed in periodic solids as a momentum-conserving process, giving the indication that it can be used as an interesting band-mapping technique.[13,20,21] The same starting point was adopted to unravel the symmetry-selective properties of RIXS in recent theoretical works focusing on molecules.[22,15,10] By means of model calculations several features of resonant x-ray scattering was proposed and analyzed and which have no counterpart in the more well-investigated nonresonant cases, such as tail excitation, form of the excitation frequency function, Stokes doubling, and state interference effects.[22,15,10] The interference of scattering channels through the core-hole states localized at different atoms was studied theoretically in Ref. 22, with the symmetry-selective character of RIXS displayed both in the localized and delocalized core-hole descriptions. It was also shown that the dipole nature of RIXS transitions imposes strong selectivity, in contrast to the nonresonant case where it "only" acts selective for local electron density, being selective in terms of a molecular-orbital (MO) analysis only in rare cases. As shown in all these investigations, the RIXS cross section depends strongly on the symmetry of the occupied and unoccupied levels, and on the frequency of the incoming photons.

The strongest frequency dependency occurs for small widths of the excitation functions; however, when linear dispersion and resonant sharpening below the lifetime width prevails, the strong frequency and shape dependence also persist for somewhat broader bandpasses of the excitation spectral functions. This dependence is quite different in the different frequency regions below the ionization threshold, i.e., the band-gap, low-energy-resonant, and high-energy-resonant regions. The two former regions show a very strong correlation between the shapes of the RIXS spectrum and the photon spectral function, while RIXS spectra pertaining to higher resonant energies exhibit less frequency dependency, and become nonresonantlike because of the higher density of core-excited states closer to the ionization threshold.

Stokes doubling or Stokes shifting is one effect that serves as a source for the strong excitation energy dependency of the RIXS spectral shape, and which now is possible to observe with current instrumentation. These effects operate over the full energy range, but are particularly conspicuous for band-gap excitation when the frequency ω of a narrow-band x-ray beam is detuned below the lowest x-ray-absorption resonance, and where a single RIXS line is shifted or even doubled. The symmetry-selective character of RIXS is the other important factor that contributes to the strong correlation between the shapes of the RIXS spectrum and the photon spectral function. It also leads to the RIXS spectra becoming very sparse in the limit of long core-hole state lifetimes and narrow-band excitation. That RIXS spectra pertaining to higher resonant energies involving a higher density of core-excited states appear nonresonantlike can be ascribed to the effects of tail excitation of (slightly) nonresonant states and of vibronic coupling between these states. These processes may even be operating at the lowest unoccupied molecular-orbital level, as here verified. On the other hand, tuning the exciting x rays to lower energies into the band-gap region, the RIXS spectrum is purified in the sense that tail excitation vanishes and that the spectra become the product of electronic symmetry-selection rules only. Thus spectra recorded in the band-gap region can potentially be used as tools for symmetry assignments of occupied levels when the symmetry of the first resonance level is known. The change, shift, and doubling of the band-gap spectra is also crucially dependent on the lifetime of the resonant core-excited states, indicating that the informational content of such spectra can be quite large.

Since the works briefly reviewed above focused on model calculations, here we use C_{60} as a far-reaching molecular case study for the application of formulations of symmetry-selective RIXS. The purpose of the present work is twofold; first, to present the high-resolution RIXS spectra of C_{60}, to analyze the spectral features, and to derive their informational contents as closely as possible; and, second, to use C_{60} with its exceptional symmetry properties to demonstrate the various consequences of RIXS theory, in particular its symmetry-related aspects. After presenting the experiment in Sec. II, and theory for symmetry-selective RIXS relevant to the present work in Sec. III, we analyze the nonresonant x-ray emission spectrum of C_{60} in Sec. IV A. Apart from a detailed assignment, we use this spectrum to calibrate the employed *ab initio* computational method, which subsequently also is applied to the RIXS spectra. Section IV B presents some preliminary aspects of the analysis of the RIXS spectrum, Sec. IV B, the computational procedures, and Sec. IV B 2 the molecular-orbital (MO) symmetries as assigned by the computations. Section IV C treats spectral intensities and shapes in RIXS spectra of C_{60}, where the different isolated properties are simulated and discussed. Symme-

try selection in RIXS, polarization and angular dependences for randomly oriented molecules, tail excitation, and vibronic coupling are analyzed in Secs. IV C 1–IV C 3. In Sec. V, the experimental results are analyzed and compared with calculations where all effects are accounted for simultaneously. Section VI summarizes the findings of the present work.

II. EXPERIMENT

The experiments were performed at beamline 7.0 of the Advanced Light Source (ALS), Lawrence Berkeley Laboratory (LBL).[23] This beamline is comprised of a 5-m, 5-cm-period undulator and a 10.000-resolving-power spherical grating monochromator (SGM) covering the spectral range from 100 to 1300 eV. The sample was made *in situ* by vacuum evaporation of pure C_{60} (99.98%) on a clean and fine Fe surface in the preparation chamber under UHV conditions. The evaporation was done by slowly increasing the temperature to ~250 °C and maintaining for outgassing, and then the film was obtained at 380 °C by 25-min evaporation. Pressure in the preparation chamber was 8.0×10^{-10} Torr before evaporation and 2×10^{-8} Torr at evaporation. The C_{60} film was then transferred from the preparation chamber into the analysis chamber at UHV condition, and the experiments were carried out at a pressure of 1.5×10^{-9} Torr. The film was thick enough so that the $L_{2,3}$ emission lines of Fe cannot be observed with 3-keV electron excitation. The near-edge x-ray-absorption spectrum showed that the C_{60} film was of good quality. The soft-x-ray fluorescence was recorded both parallel and perpendicular to the polarization of the incoming x-ray photon beam; i.e., both horizontally and vertically using a high-resolution grazing-incidence grating spectrometer with a two-dimensional detector.[24,25] The bandpass of the incoming photon beam was set to 0.15 and 0.22 eV, respectively, for x-ray absorption spectroscopy (XAS) and x-ray emission spectroscopy (XES) measurements, and the spectrometer resolution was about 0.5 eV. The energy scale in the x-ray emission spectra was calibrated by using the elastic peak and Cu $L_{2,3}$ emission lines recorded in the third order of diffraction.

III. THEORY FOR RESONANT INELASTIC X-RAY SCATTERING

The interaction of light with electrons can be described in terms of the perturbing Hamiltonian

$$H_{\rm int}=\tfrac{1}{2}\sum_i[-\alpha(\mathbf{p}_i\cdot\mathbf{A}+\mathbf{A}\cdot\mathbf{p}_i)+\alpha^2\mathbf{A}\cdot\mathbf{A}]\ , \tag{1}$$

where $\mathbf{A}$ is the quantized radiation field in the point $\mathbf{r}_i$, and $\mathbf{p}_i$ the momentum operator of the ith electron. We use atomic units ($\hbar=m=e=1,\alpha=\frac{1}{137}$), which uncover some crucial properties of the electron-radiation interaction $H_{\rm int}$. The interaction is small for moderate x-ray intensities due to the smallness of the fine-structure constant: $\alpha\sim10^{-2}$, thus validating the use perturbation theory. As shown by the quantum-mechanical (quantized) theory of the interaction of light and matter (see, e.g., Ref. 26), the interaction term $-\alpha(\mathbf{p}_i\cdot\mathbf{A}+\mathbf{A}\cdot\mathbf{p}_i)$ can only mediate one-photon effects; that is, absorption or emission of single photons in the first order of perturbation theory. It thus makes no first-order contribution to a scattering process in which there is no net change in the number of photons, but it can contribute by considering second-order perturbation theory over α. The expansion of $H_{\rm int}$ shows that the interaction $\alpha^2\mathbf{A}\cdot\mathbf{A}$ must be taken into account in the first order of perturbation theory. The interaction $\alpha^2\mathbf{A}\cdot\mathbf{A}$ can lead to the simultaneous absorption or emission of two photons. Therefore, it makes nonvanishing contributions to a scattering process in the first order already. However, for the soft-x-ray wavelength region, higher terms in the expansion of $A_0e^{i\mathbf{k}\cdot\mathbf{r}_i}=A_0+A_0\mathbf{k}\cdot\mathbf{r}_i+\cdots$ are small. This is so because $\mathbf{k}\cdot\mathbf{r}_i\approx r_i/\lambda$, and λ is much larger than the typical dimension of the electron clouds in atoms or molecules. In the dipole approximation with constant $\mathbf{A}$ across the electron range no contributions will result from the $\mathbf{A}\cdot\mathbf{A}$ term for a scattering that changes the molecular states involved. The quadratic term $\mathbf{A}\cdot\mathbf{A}$ thus makes contributions only to the elastic scattering amplitude, and, in the dipole approximation, the inelastic scattering amplitude receives contributions only from the interaction term $(\mathbf{p}_i\cdot\mathbf{A}+\mathbf{A}\cdot\mathbf{p}_i)$ through second-order perturbation theory.

The total x-ray scattering amplitude is described by the Kramers-Heisenberg formula[26]

$$F_{\nu n}(\omega,\omega')=F_{\nu n}(\omega)+F_{\nu n}^{\rm NR}(\omega')=\sum_k f_{\nu n}^k(\omega)+F_{\nu n}^{\rm NR}(\omega')\ , \tag{2}$$

$$f_{\nu n}^k(\omega)=\alpha\omega_{\nu k}\omega_{nk}(\nu)\frac{(\mathbf{d}_{\nu k}\cdot\mathbf{e}_1)[\mathbf{e}_2\cdot\mathbf{d}_{kn}(\nu)]}{\omega-\omega_{\nu k}+i\Gamma_{\nu k}}\ , \tag{3}$$

and

$$F_{\nu n}^{\rm NR}(\omega')=\alpha(\mathbf{e}_2\cdot\mathbf{e}_1)\delta_{\nu n}-\alpha\sum_k\omega_{\nu k}\omega_{nk}(\nu)\frac{(\mathbf{e}_2\cdot\mathbf{d}_{\nu k})[\mathbf{d}_{kn}(\nu)\cdot\mathbf{e}_1]}{\omega'+\omega_{\nu k}}\ . \tag{4}$$

where $\mathbf{d}_{\nu k}=\langle0|\sum_i\mathbf{r}_i|k^{-1}\nu\rangle$ and $\mathbf{d}_{kn}(\nu)=\langle k^{-1}\nu|\sum_i\mathbf{r}_i|n^{-1}\nu\rangle$ are dipole matrix elements of x-ray-absorption ($k\rightarrow\nu$) and emitted ($n\rightarrow k$) transitions, respectively. Indices k, n, and ν denote levels defined by core, occupied, and unoccupied molecular orbitals, respectively. ω,ω' and $\mathbf{e}_1,\mathbf{e}_2$ are the frequencies and polarization vectors of incoming and emission photons: $\omega_{\nu k}=E(k^{-1}\nu)-E_0,\omega_{nk}(\nu)=E(k^{-1}\nu)-E(n^{-1}\nu)$. $\omega_{\nu n}=E(n^{-1}\nu)-E_0$ is a frequency for the optical excitation $n\rightarrow\nu$ and is equal to the difference between energies $E(n^{-1}\nu)$ and E_0 of excited $|n^{-1}\nu\rangle$ and ground $|0\rangle$ molecular states; $\Gamma_{\nu k}$ is the half width at half-maximum (HWHM) of the x-ray-absorption line $k\rightarrow\nu$. The polarization vectors will be expressed in lab coordinates X, Y, and Z, the dipole matrix elements in molecular coordinates x', y', and z'; see Fig. 1. The electron excited to the vacant MO ψ_ν screens differently the subsequent decay of

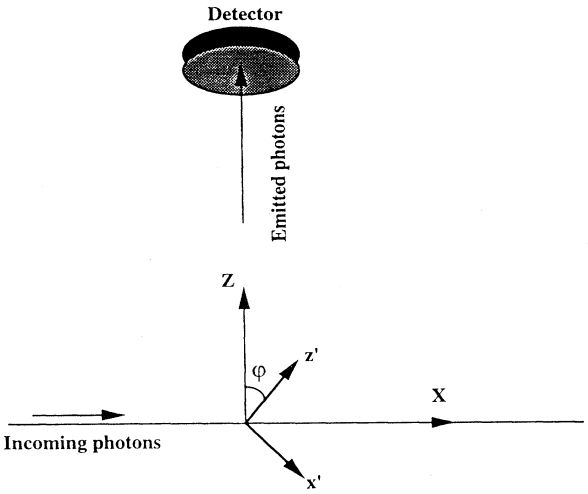

FIG. 1. Laboratory (X,Y,Z) and molecular (x',y',z') axes.

electrons from various occupied levels n to the inner shell k. This specific screening effect leads to a dependence on ν of the frequencies $\omega_{nk}(\nu)$ and the dipole matrix elements $\mathbf{d}_{kn}(\nu)$. The Kramers-Heisenberg formula describes both x-ray elastic $(\nu=n)$ and inelastic $(\nu\neq n)$ scattering.

The term $F_{\nu n}(\omega)$ given by Eq. (3) shows a strong resonant effect when the condition $\omega=\omega_{\nu k}$ is fulfilled, and is usually called the resonant anomalous scattering term. The nonresonant scattering amplitude $F_{\nu n}^{\mathrm{NR}}(\omega')$ consists of two terms. The first one is the elastic scattering amplitude ($\propto\delta_{\nu n}$) caused by the ($\mathbf{A}\cdot\mathbf{A}$) term, while the second contribution is caused by the ($\mathbf{p}_i\cdot\mathbf{A}+\mathbf{A}\cdot\mathbf{p}_i$) term. The nonresonant scattering is important only far from resonance (for example, in the cases of Raleigh or Thompson scattering). The ratio of the nonresonant amplitude $F_{\nu n}^{\mathrm{NR}}(\omega')$ to the resonant one $F_{\nu n}(\omega)$ (in exact resonance) is of the order $r_0/\lambda\ll 1$.[26] Here $r_0\simeq 2.8\times 10^{-13}$ cm is the classical radius of the electron and $\lambda\sim 10^{-6}$–10^{-7} cm is the wavelength of the x-ray photon. Only the x-ray resonant scattering will be investigated in this paper, experimentally and theoretically. Therefore, we will ignore the small nonresonant term $P_{\nu n}^{\mathrm{NR}}(\omega')$ in the Kramers-Heisenberg formula [see Eqs. (2), (3), and (4)].

The spectral and polarization properties of the resonant x-ray scattering are guided by the double-differential cross section,[26,22,15]

$$\frac{d^2\sigma}{d\omega' d\Omega}=\frac{d^2\sigma^{\mathrm{RIXS}}}{d\omega' d\Omega}+\frac{d^2\sigma^{\mathrm{REXS}}}{d\omega' d\Omega}\ , \tag{5}$$

which is the sum of the double-differential cross sections of resonant inelastic x-ray scattering (RIXS) $(\nu\neq n)$

$$\frac{d^2\sigma^{\mathrm{RIXS}}}{d\omega' d\Omega}=\sum_{\nu}\sum_{n}\frac{\omega'}{\omega}|F_{\nu n}(\omega)|^2\Delta(\omega-\omega'-\omega_{\nu n},\Gamma_{\nu n})\ , \tag{6}$$

and resonant elastic x-ray scattering (REXS) $(\nu=n)$

$$\frac{d^2\sigma^{\mathrm{REXS}}}{d\omega' d\Omega}=\frac{\omega'}{\omega}\left|\sum_{\nu}F_{\nu\nu}(\omega)\right|^2\delta(\omega-\omega')\ . \tag{7}$$

There are two principal distinctions between REXS (7) and RIXS (6) cross sections. The first is connected with the lifetime of the final state. For the elastic case this state is the ground state with infinite lifetime which leads to infinite narrow REXS lines described by the Dirac δ function $\delta(\omega-\omega')$. In the case of inelastic scattering the final state is an optically excited state $n\rightarrow\nu$ with finite lifetime $\Gamma_{\nu n}^{-1}$. Thus the RIXS spectral lines are broadened by the Lorentzian spectral function

$$\Delta(\omega,\Gamma)=\frac{\Gamma}{\pi(\omega^2+\Gamma^2)}\ . \tag{8}$$

The lifetime broadening $\Gamma_{\nu n}$ of the optical transition $n\rightarrow\nu$ is negligibly small in comparison with the width of x-ray transitions $\Gamma_{\nu k}$. This allows us to use $\Gamma_{\nu n}=0$ and to replace the Δ function (8) in Eq. (6) by the Dirac δ function $\delta(\omega-\omega'-\omega_{\nu n})$. This circumstance is the basis for super-high-resolution x-ray spectroscopy, and allows the recording of x-ray fluorescence resonances without lifetime broadening.[11,14,16] In this paper we will neglect the final-state lifetime broadening $\Gamma_{\nu n}=0$. The qualitatively different role of the unoccupied levels ν in REXS and RIXS cross sections is the second important distinction between these processes. As seen from Eq. (7), the elastic-scattering cross section is the square of the sum of partial scattering amplitudes $|\sum_{\nu}F_{\nu\nu}|^2$, while the inelastic scattering cross section (6) is the sum of the partial cross sections $\sum_{\nu n}|F_{\nu n}|^2$. The reason for this is that, contrary to RIXS, the level ν is intermediate in the REXS process, with the result that the interference between scattering channels with different ν takes place.[15] For the close-lying unoccupied ν levels this interference causes a violation of the two-step model.

From now on we focus on the RIXS process, and drop for brevity its subscript: $\sigma(\omega',\omega)\equiv\sigma^{\mathrm{RIXS}}(\omega',\omega)$. To describe a realistic experimental situation, we must use the convolution

$$\begin{aligned}\sigma(\omega',\omega_0)&=\int d\omega\frac{d^2\sigma}{d\omega' d\Omega}\Phi(\omega-\omega_0)\\&=\sum_{\nu n}\frac{\omega'}{\omega}|F_{\nu n}(\omega)|^2\Phi(\omega'+\omega_{\nu n}-\omega_0)\end{aligned} \tag{9}$$

of the cross section (6) with the incoming photon distribution function $\Phi(\omega-\omega_0)$ centered at frequency ω_0. The width of the convolution lines is restricted only by the width γ of the spectral function Φ of incoming x rays and, of course, by the instrumental resolution. The frequency ω' of the emitted x-ray photons has a Raman-related shift (Stokes shift) into the long-wave region relative to the frequency ω of the absorbed photon

$$\omega=\omega'+\omega_{\nu n}\ , \tag{10}$$

in accordance with the energy conservation law reflected by the $\delta(\omega-\omega'-\omega_{\nu n})$ function.

The dipole moments $\mathbf{d}_{\nu k}$ and $\mathbf{d}_{kn}$ will be expressed in laboratory coordinate axes through the directional cosine transformation $T_k^X=T_k^{\xi}t_{\xi X}+T_k^{\eta}t_{\eta X}+T_k^{\zeta}t_{\zeta X}=T_k^{\alpha}t_{\alpha X}$, where the repeated Greek index α implies a summation over the values ξ, η, and ζ. $t_{\xi X}$ is the cosine of the angle

between the ξ axis of the molecular coordinate system and the X axis of the laboratory coordinate system. The eight other directional cosines $t_{\xi Y}$, $t_{\xi Z}$, $t_{\eta X}$, . . . are named similarly; the general direction cosine $t_{\alpha A}$ has a Greek letter for the molecular axis and a capital italic letter for the laboratory axis. Putting this into Eq. (2), we obtain

$$F_{\nu n}=\alpha\sum_k \omega_{\nu k}\omega_{nk}(\nu)\left[\frac{d^{\beta}_{\nu k}t_{\beta A}e^{*}_{1A}d^{\gamma}_{kn}(\nu)t_{\gamma B}e_{2B}}{\omega'-\omega_{nk}+i\Gamma_{\nu k}}\right] \quad (11)$$

or, rearranging, as

$$F_{\nu n}=(t_{\beta A}t_{\gamma B})(e^{*}_{1A}e_{2B})F^{\beta\gamma}_{\nu n} , \quad (12)$$

where we denote

$$F^{\beta\gamma}_{\nu n}=\alpha\sum_k \omega_{\nu k}\omega_{nk}(\nu)\left[\frac{d^{\beta}_{\nu k}d^{\gamma}_{kn}(\nu)}{\omega'-\omega_{nk}+i\Gamma_{\nu k}}\right] \quad (13)$$

as the RIXS transition element. It can be seen that $F^{\beta\gamma}_{\nu n}$ is a tensor of second rank. The quantity $|F_{\nu n}|^2$ is thus written as

$$|F_{\nu n}|^2=(e^{*}_{1A}e_{2B}e_{1R}e^{*}_{2S})[t_{\beta A}t_{\gamma B}t_{\rho R}t_{\sigma S}](F^{\beta\gamma}_{\nu n}F^{\rho\sigma *}_{\nu n}) . \quad (14)$$

All polarization information is collected in the first factor, all molecular information in the last factor, and all orientational information in the middle factor. Both the first and last factors are Cartesian tensors of the fourth rank. For molecules with a fixed orientation, such as surface adsorbates, one can use two of these factors to derive information about the third; e.g., knowing the polarization and sample orientation, the RIXS spectrum allows a symmetry assignment of electronic states, or vice versa, from the knowledge of the polarization of radiation and the symmetries of the states involved in RIXS, the orientation of the sample can be derived. In the case of gas-phase samples, averaging must be employed. Only the orientational factor needs averaging; the polarization and symmetry factors are independent of orientation. The polarization dependence of the RIXS transitions makes it possible to assign the symmetry of the occupied and unoccupied molecular orbitals.

A. Randomly oriented molecules

A detailed description of the procedure for orientational averaging referring to the case of randomly oriented molecules can be found in our previous study[10] (see also the work of McClain[27] for general two-photon transitions). It gives

$$\langle |F_{\nu n}|^2\rangle=\lambda_{\nu n}=F\lambda^{F}_{\nu n}+G\lambda^{G}_{\nu n}+H\lambda^{H}_{\nu n} , \quad (15)$$

with

$$\lambda^{F}_{\nu n}=\sum_{\beta}F^{\beta\beta}_{\nu n}\sum_{\gamma}F^{\gamma\gamma *}_{\nu n}=\left|\sum_k \zeta^{k}_{\nu n}\cos\varphi^{kk}_{\nu n}\right|^2 , \quad (16)$$

$$\lambda^{G}_{\nu n}=\sum_{\beta}F^{\beta\gamma}_{\nu n}F^{\beta\gamma *}_{\nu n}=\sum_{kk_1}\zeta^{k*}_{\nu n}\zeta^{k_1}_{\nu n}\cos\varphi^{kk_1}_{\nu\nu}\cos\varphi^{kk_1}_{nn} , \quad (17)$$

$$\lambda^{H}_{\nu n}=\sum_{\beta\gamma}F^{\beta\gamma}_{\nu n}F^{\gamma\beta *}_{\nu n}=\sum_{kk_1}\zeta^{k*}_{\nu n}\zeta^{k_1}_{\nu n}\cos\varphi^{kk_1}_{\nu n}\cos\varphi^{k_1k}_{\nu n} . \quad (18)$$

λ functions are expressed through the angle $\varphi^{kk_1}_{ij}$ between transition dipole moments $\mathbf{d}_{ik}$ and $\mathbf{d}_{jk_1}$,

$$\cos\varphi^{kk_1}_{ij}=\frac{\mathbf{d}_{ik}\cdot\mathbf{d}_{jk_1}}{d_{ik}d_{jk_1}} , \quad (19)$$

for the case of real dipole moments. Here

$$\zeta^{k}_{\nu n}=\frac{\alpha\omega_{\nu k}\omega_{nk}(\nu)}{\omega'-\omega_{nk}+i\Gamma_{\nu k}}d_{\nu k}d_{kn} . \quad (20)$$

The cross terms $\zeta^{k*}_{\nu n}\zeta^{k}_{\nu n}$ in Eqs. (16), (17), and (18) describe the interference of scattering channels through the different core levels $k\neq k_1$. This interference is a characteristic feature of the one-step description, which has been neglected in the two-step model. The F, G, and H factors are

$$F=-|\mathbf{e}_1\cdot\mathbf{e}_2|^2+4|\mathbf{e}_1^{*}\cdot\mathbf{e}_2|^2-1 , \quad (21)$$

$$G=-|\mathbf{e}_1\cdot\mathbf{e}_2|^2-|\mathbf{e}_1^{*}\cdot\mathbf{e}_2|^2+4 , \quad (22)$$

$$H=4|\mathbf{e}_1\cdot\mathbf{e}_2|^2-|\mathbf{e}_1^{*}\cdot\mathbf{e}_2|^2-1 . \quad (23)$$

The averaged cross section is given in terms of these factors as

$$\begin{aligned}\langle\sigma(\omega',\omega_0)\rangle&=\sum_{\nu n}\frac{\omega'}{\omega}\lambda_{\nu n}\Phi(\omega'+\omega_{\nu n}-\omega_0)\\&=\sum_{\nu n}\frac{\omega'}{\omega}(F\lambda^{F}_{\nu n}+G\lambda^{G}_{\nu n}+H\lambda^{H}_{\nu n})\\&\quad\times\Phi(\omega'+\omega_{\nu n}-\omega_0) .\end{aligned} \quad (24)$$

These expressions show that the RIXS cross section in general depends strongly on the polarization vectors of absorbed and emitted photons, and on the symmetries of the unoccupied and occupied MO's. Equation (24) is perfectly general for photons of linear, circular, or elliptical polarization.

The parity and symmetry selection rules for the RIXS transitions have been discussed in our previous studies.[22,10] In general, the selection rule is controlled by the parameter $d^{\beta}_{\nu k}d^{\gamma}_{kn}(\nu)$. For instance, if occupied and unoccupied MO's have opposite parities, ug or gu, then $d^{\beta}_{\nu k}d^{\gamma}_{kn}(\nu)\equiv 0$, and the transition is forbidden. Using group theory it is also possible to give the symmetry-selection rule for the RIXS process; the product of irreducible representations $\Gamma_\nu\times\Gamma_\alpha\times\Gamma_\beta\times\Gamma_n$, where ν and n denote unoccupied and occupied orbitals, and α and β dipole moment components, must contain the totally symmetric representation.

The molecular parameters $\lambda^{F}_{\nu n}$, $\lambda^{G}_{\nu n}$, and $\lambda^{H}_{\nu n}$ are dependent on the symmetries of the unoccupied, ν, and occupied, n, MO's. For orbitals with different symmetries, the polarization dependences will not be the same. Polarized RIXS thus provides a useful tool for assignments of the occupied and unoccupied MO's. The polarization vectors may be real, representing linearly polarized photons, or complex, representing circularly or elliptically polarized photons. If we denote the angle between the linear polarization vectors of absorbed and emitted photons by

angle θ, the square of the scattering amplitudes will be expressed as

$$\lambda_{\nu n}=(-\lambda^F_{\nu n}+4\lambda^G_{\nu n}-\lambda^H_{\nu n}) +(3\lambda^F_{\nu n}-2\lambda^G_{\nu n}+3\lambda^H_{\nu n})\cos^2\theta\ . \quad (25)$$

This formula has the same content as Eq. (13) in the work of Gel'mukhanov and Ågren.[22] Such a formula is an exact prediction of the linear polarization behavior of the RIXS cross section. This polarization dependence is in general quite strong. For experimental reasons the polarizations of both incoming and outgoing photons are not often determined (see, however, experiments by Lindle *et al.*[28] and Southworth *et al.*[29]), and the cross section is obtained either as angular dependent for unpolarized incoming photons, or as dependent on the polarization of the incoming photons for a fixed exit angle. It is necessary to replace $\cos^2\theta$ with $\frac{1}{2}\sin^2\chi$ for the two latter situations, i.e., when the initial x-ray beam is unpolarized or when a summation over the final photon polarization vectors $\mathbf{e}'$ is made. In the first case χ is the angle between $\mathbf{e}'$ and the direction $\mathbf{n}$ of incoming photon propagation, and in the second case χ is the angle between $\mathbf{e}$ and $\mathbf{n}'$, the direction of the outgoing photon propagation.

The polarization parameter P is defined as the ratio between different RIXS cross sections for different combinations of photon polarization vectors, and can be directly measured experimentally. Many different combinations of polarization vectors of absorbed and emitted photons can be formed. However, basically one needs at least three of these combinations, two of them involving circular polarization vectors. We label the RIXS cross sections as $\lambda_{\nu n}(lp)$, $\lambda_{\nu n}(ln)$, and $\lambda_{\nu n}(cp)$ for two absorbed and emitted photons having parallel linear, perpendicular linear, and parallel circular polarizations, respectively. The latter can be arbitrarily clockwise or counterclockwise. The polarization ratios can then be written as

$$P1=\frac{\lambda_{\nu n}(ln)}{\lambda_{\nu n}(lp)}=\frac{-\lambda^F_{\nu n}+4\lambda^G_{\nu n}-\lambda^H_{\nu n}}{2\lambda^F_{\nu n}+2\lambda^G_{\nu n}+2\lambda^H_{\nu n}}\ , \quad (26)$$

$$P2=\frac{\lambda_{\nu n}(cp)}{\lambda_{\nu n}(lp)}=\frac{-2\lambda^F_{\nu n}+3\lambda^G_{\nu n}+3\lambda^H_{\nu n}}{2\lambda^F_{\nu n}+2\lambda^G_{\nu n}+2\lambda^H_{\nu n}}\ , \quad (27)$$

$$P3=\frac{\lambda_{\nu n}(cp)}{\lambda_{\nu n}(ln)}=\frac{-2\lambda^F_{\nu n}+3\lambda^G_{\nu n}+3\lambda^H_{\nu n}}{-\lambda^F_{\nu n}+4\lambda^G_{\nu n}-\lambda^H_{\nu n}}\ . \quad (28)$$

By measuring the polarization ratios $P1$, $P2$, and $P3$, it is possible to assign the symmetries of occupied or unoccupied MO's. A detailed discussion concerning the symmetry assignments of electronic states from the polarization ratios for any of the 32 crystallographic groups can be found in Ref. 10.

B. Spectral shape and Stokes doubling

It is a reasonable approximation to assume that for a fixed ν MO, the core-excited state lifetime broadening $\Gamma_{\nu k}$ is the same for all core-excited states (core MO's k), i.e., $\Gamma_{\nu k}=\Gamma_{\nu 0}$. Since symmetry-adapted core orbitals for a molecule such as C_{60} are quasidegenerate, one could further assume that $\omega_{nk}=\omega_{n0}$ for all core MO's k. This should be a good approximation at least for first-row species which lack spin-orbit or molecular-field splittings of the core levels. Doing so, $F^{\beta\gamma}_{\nu n}$ in Eq. (13) can simply be written as $F^{\beta\gamma}_{\nu n}\propto(\omega'-\omega_{n0}+i\Gamma_{\nu 0})^{-1}$. By inspecting the definition for the cross section, Eqs. (24), we can see that the spectral shape of the RIXS spectrum is determined by the function

$$\Xi(\Omega)=\Delta(\Omega,\Gamma)\Phi(\Omega-\Omega_0)\ , \quad (29)$$

where $\Omega_0=\omega_0-\omega_{\nu 0}$ and $\Omega=\omega'-\omega_{n0}(\nu)$ are the frequency detunings from absorption and emission resonances, respectively. The $\Delta(\Omega,\Gamma)$ function responsible for emission leads to the ordinary condition for an emission resonance:

$$\Omega=0\ . \quad (30)$$

At the maximum of the incoming x-ray spectral function $\Phi(\Omega-\Omega_0)=\Delta(\Omega-\Omega_0)$, the detunings of both incoming and outgoing photons are the same:

$$\Omega=\Omega_0\ . \quad (31)$$

This condition, describing the energy conservation law [Eq. (10)], gives a Stokes shift of the photon frequency under the RIXS process. The spectral shape described by function (29) has two resonant features, (30) and (31). This results in a doubling of the ordinary RIXS lines, a Stokes doubling. Recently this effect was investigated for nonradiative (Auger) x-ray Raman scattering in Refs. 30 and 31. The intensity ratio of the Stokes (31) and the normal RIXS (30) lines is governed by the width ratio $\xi=\Gamma/\Gamma_\Phi$, as can be seen from Eq. (29). One can easily understand that the Stokes doubling of the normal RIXS line is not always observable. Indeed, conditions (30) and (31) can often only lead to one resonance feature with an asymmetrical spectral shape. The strict conditions for the Stokes doubling effect depend strongly on the shape of the spectral function $\Phi(\Omega-\Omega_0)$. As the most important limiting case we approximate the spectral function $\Phi(\Omega-\Omega_0)$ of incoming x-ray photons by a Gaussian $[\Phi(\Omega)\propto\exp(-(\Omega/\Gamma_\Phi)^2)]$. Stokes doubling of RIXS lines can then take place only in the narrow energy region indicated in Fig. 2. For Gaussian band shapes there is a lower limit for the width with respect to the lifetime broadening Γ of the normal RIXS line ($\Gamma_\Phi/\Gamma>\sqrt{8}$). This condition leads to that the width of the normal RIXS resonance always is smaller than the width of the Stokes resonance and is approximately equal to the lifetime broadening Γ, cf. Fig. 3. This analysis provides an easy clue as to how the experimental parameters should be tuned in order to find Stokes doubling effects. In general cases we have to simulate directly the effects of the full cross-section formulas (9) or (24) and take into account interfering effects of overlapping RIXS lines.

IV. RESULTS AND DISCUSSIONS

A. Nonresonant x-ray emission spectrum of C_{60}

It is relevant to start a discussion of the resonant inelastic scattering spectrum of C_{60} by analyzing the non-

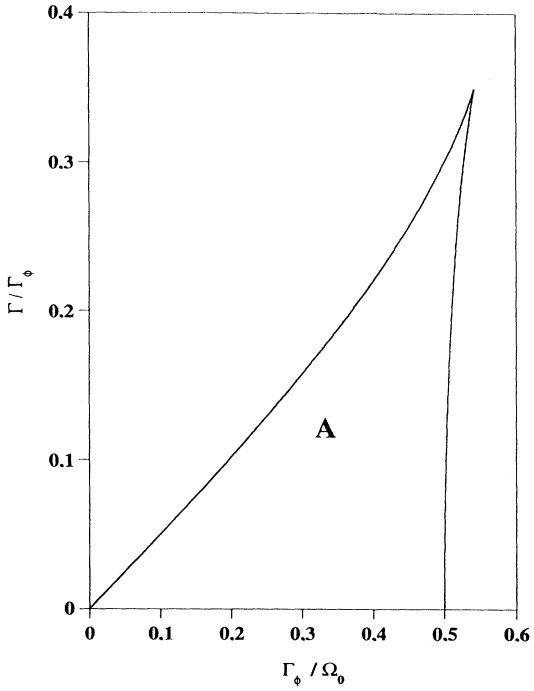

FIG. 2. Limiting conditions for observing Stokes doubling in RIXS spectra. The region for the Stokes doubling effect is denoted by symbol *A*. A Gaussian spectral function is assumed.

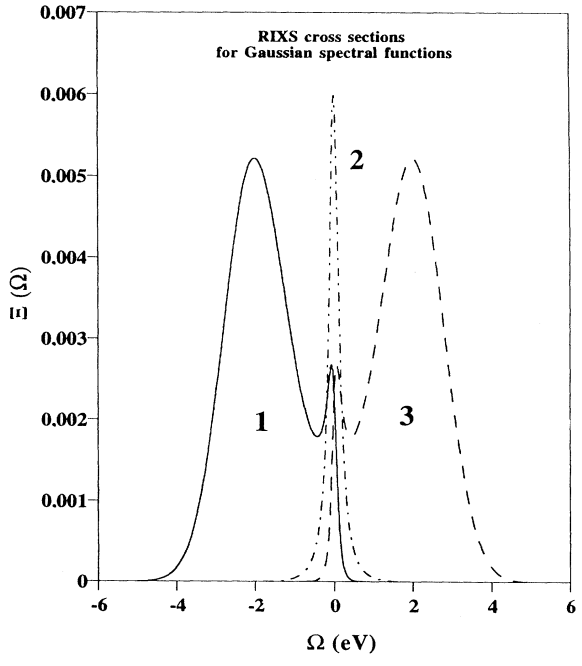

FIG. 3. Stokes doubling of RIXS lines for different forms of the excitation spectral function. A Gaussian spectral function is assumed: $\Gamma=0.15$ eV, $\Gamma_\Phi=1$ eV. (1) $\Omega_0=-2.5$ eV. (2) $\Omega_0=0$ eV. (3)$\Omega_0=2.5$ eV. Curve 2 is reduced 200 times.

resonant x-ray spectrum first. The strict symmetry-selection rules imposed by the dipole nature of the soft-x-ray radiation, and the one-center decomposition model (local symmetry-selection rules) have constituted the two main tools in the analysis of such nonresonant spectra. The strict symmetry-selection rule is most powerful for the case of degenerate or nondegenerate core orbitals localized at inversion centers, or with atomic quasidegenerate core orbitals split by molecular fields, SF_6 and CO_2 being two important examples, while it is somewhat less selective in the more common classes of molecules with multicenter core orbitals delocalized over symmetry-related atoms, such as N_2, C_6H_6, and C_{60}. Actually, even for a molecule of very high symmetry like C_{60}, the strict symmetry selection does not as such make it possible to assign symmetries because all orbitals remain allowed. This is in sharp contrast to the resonant case, as shown in Sec. IV B.

The x-ray emission spectrum of the C_{60} molecule was recently analyzed by *ab initio* Hartree-Fock calculations with standard single- (SZ), double- (DZ), and triple-zeta (TZ) basis sets.[9] The results with the TZ basis set are recapitulated in Fig. 4, together with the experimental spectra obtained with 3-keV electron-beam and synchrotron radiation (400-eV photon energy) excitation.[32] The frozen orbital model with many-center transition moments in the full I_h symmetry were obtained over all, quasidegenerate, 60 core orbitals and the 120 occupied valence orbitals. The dependence of the x-ray emission intensities on the size of the applied basis sets indicated that the obtained large basis set results provide a good representation of the one-particle x-ray emission spectrum of C_{60}, and an assignment of the structures in the experimental spectrum was thereby accomplished, as shown in Fig. 4. For example, it was found that the first three highest occupied valence orbitals have h_u, h_g, and g_g symmetries, respectively, which is in agreement with the assignments of Refs. 33 and 34, and which also agree with the experimental assignments of Weaver *et al.*[1] However, for other orbitals, the assignments based on the nonresonant x-ray spectrum were different from earlier calculations.[33,35]

The calculations in Ref. 9 predicted the one-particle spectrum and excluded relaxation and correlation effects. Earlier experience indicates that the calculated relative intensities within the frozen orbital approximation are in quite fair agreement with experiment.[36] Frozen orbital energies generally give the correct ordering of ionization energies for outer valence levels of small molecules. The relaxation energies as obtained from ΔSCF (self-consistent-field) calculations have been found to vary only moderately.[37] For larger systems, *ab initio* Hartree-Fock calculations generally exaggerate the total width of the valence band due to the neglect of electron correlation,[34,38–41] and this seems to be the case for C_{60} as well. This wideness stems from the correlation error of binding energies of deeper valence orbitals in such systems. After division of a factor of 1.3 [a factor widely accepted in the studies for larger polymer systems,[34,39–41] and also used in investigations of the valence electron structure of C_{60} (Ref. 34)], a very good intensity distribution for the non-

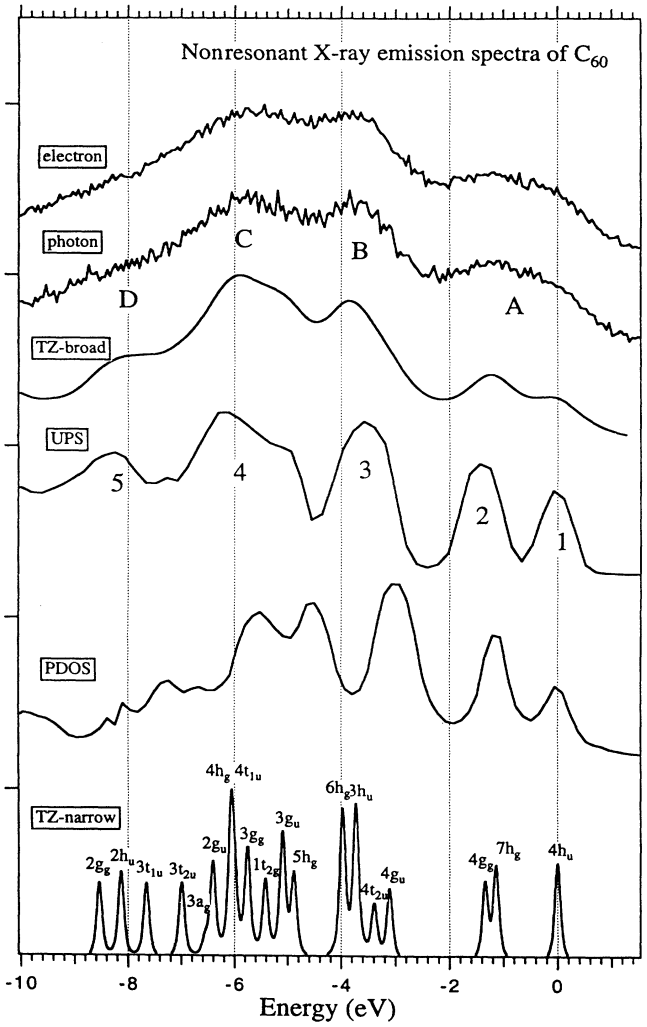

FIG. 4. Nonresonant x-ray emission spectra of C_{60}.

resonant x-ray spectrum of C_{60} was obtained from the frozen orbital calculations. This fact is of importance for the computational analysis of the corresponding RIXS spectra given below. This also indicates that the electronic structure of the fullerenes is only slightly affected by solidification. From the experimental agreement a rather detailed assignment of the nonresonant spectrum can be proposed: Feature *A* is produced by the first three highest occupied orbitals $4h_u$, $7h_g$, and $4g_g$, which agree with the assignment of photoemission spectra of Weaver *et al.*[1] and the partial-density-of-states (PDOS) calculation in Ref. 33. Feature *B* has been assigned as g_u, h_u, h_g, and t_{2u} states by the PDOS calculations.[33] The x-ray calculations indicate that this feature is due mainly to contributions from the $6h_g$ and $3h_u$ states, showing large transition intensities, while the $4g_u$ and $4t_{2u}$ states make relatively small contributions. Feature *C* seems to have contributions from several states, possibly from two h_g, one g_g, two g_u, one t_{1u} and one t_{2g} states. The $3t_{1u}$, $2h_u$, and $2g_g$ states would then be the main contributor to feature *D*.

States with *h* symmetries make large contributions to the x-ray emission spectrum, which to some extent could refer to the large degeneracy of these $2p$-containing orbitals. The full transition moments compare quite well with the *p* density of states of the high-energy part, but somewhat worse for the low-energy part, which can be taken as an indication that cross *s-p* and *p-p* contributions are important in addition to the one-center *s-p* contributions. The latter are taken into account by the *p*-density-of-states and the one-center intensity models. As noted in Ref. 9, the comparison with the ultraviolet photoemission spectroscopy (UPS) spectrum indicates a rather striking similarity between predicted XES structures and measured UPS structures. The main experimental features of the nonresonant x-ray spectrum labeled with *A*, *B*, *C*, and *D* thus correspond to features of 1, 2, 3, 4, and 5 labeled in the photoemission spectra of Weaver *et al.*[1] This supports a density-of-state interpretation, i.e., that the number of states per unit energy interval and the degree of degeneracy are more important factors than the matrix elements.

B. Resonant inelastic x-ray scattering spectra of C_{60}

1. *Calculations*

The resonant elastic and inelastic spectra of C_{60} are obtained at the same approximation level as the nonresonant spectrum discussed in Sec. IV A, thus from Hartree-Fock frozen orbital calculations, with all-center x-ray transition moments obtained in the full I_h symmetry. The TZ basis set was used, which in the nonresonant case gave results almost identical to the DZ basis. This fact, and the successful assignment of the nonresonant spectrum using *ab initio* Hartree-Fock calculations, indicates that the deexcitation part of the RIXS process should be well reproduced by orbital energies and transition moments obtained at the frozen orbital Hartree-Fock level. As discussed above, the one-particle spectrum of C_{60} and other "large" systems are too wide as the result of a progressive increase in the role of electron correlation down the spectrum, and we therefore employ the same compensation factor of 1.3 in the RIXS plots as in the plots for the nonresonant case. On the other hand Hartree-Fock virtual orbital energies are often poor for predicting the band-gap energies (they correspond to an *N*-electron potential), and the lowest unoccupied molecular-orbital (LUMO) energy is therefore normalized to the measured energy for the maximum of the first peak in x-ray absorption spectroscopy. Energies of other unoccupied molecular orbitals obtained from this procedure are actually found to be in reasonable agreement with the experimental values obtained with x-ray absorption spectroscopy. The RIXS band shapes are extremely dependent on the precise setting of the LUMO energies, cf. the discussion in Sec. IV C 3, and the choice between computed and experimental core absorption energies can be crucial for the final assignments of the RIXS spectra.

2. *Symmetries of occupied and unoccupied molecular orbitals*

The symmetries of occupied molecular orbitals were assigned in the study of the nonresonant x-ray emission spectra, discussed in Sec. IV A. We find the relevant unoccupied molecular orbitals governing the absorption spectrum to be of t_{1u}, t_{1g}, t_{2u}, h_g, h_u, a_g, and g_g symmetries. Four relatively strong absorption peaks have been found in the x-ray absorption spectrum. The first three have contributions from the first four LUMO orbitals (in the following denoted as the LUMO, LUMO+1, and LUMO+2 orbitals), and correspond, in order, to the t_{1u}, t_{1g}, t_{2u}, and h_g molecular-orbital symmetries. The two latter levels are energetically nearly degenerate, with h_g providing the relatively larger part of the intensity to the corresponding, unresolved, band. The fourth absorption band corresponds to the unoccupied orbitals with symmetries h_u, t_{1u}, a_g, and g_g, where h_u dominates.

C. Spectral intensities and shapes of RIXS from C_{60}

In order to describe the intensity distribution and spectral shapes in resonant x-ray scattering spectra as given by Eq. (24) one has, in addition to pure electronic factors such as symmetry selection, transition moments, and energies for individual transitions, also to consider several other factors which are particular to the RIXS process. Some of these lead only to trivial broadenings of the bands, such as vibronic excitations in the emission (Franck-Condon factors), and instrumental-related broadenings, which will not be considered in the following analysis. The nontrivial factors we discuss here are the lifetime interference effects, Stokes doubling and shifts, tail excitation, polarization and angular dependences, vibronic coupling, and hole localization. The polarization dependence is explored for randomly oriented species. Using *ab initio* data for transition moments and molecular-orbital energies as discussed above, we have simulated the RIXS spectra with respect to these different factors and with respect to different experimental conditions. For each condition, four different spectra are analyzed for which the incoming photon energies have been tuned resonant to the LUMO, LUMO+1, LUMO+2+3, and LUMO+4 levels, respectively. If not otherwise stated, the following simulations refer to cases when both incoming and emitted photons are assumed to have parallel linear polarization. The lifetime broadening of the core-excited states and the linewidths of incoming photons have strong influences on the intensities and spectral shapes of the RIXS spectra, as will be shown below. The linewidths of the incoming photons are adjusted experimentally. If not otherwise stated, the simulated RIXS spectra have been obtained for the lifetime width of 0.15 eV for all core levels, and assuming Gaussian shapes for the spectral function of the incoming photons.

1. *Symmetry selection in RIXS*

Figure 5 shows calculated RIXS spectra excited with a very small, 0.05 eV, of the spectral function for the incoming photons, together with the nonresonant, normal, x-ray emission spectrum. With this small linewidth, the effect of *tail excitation* is effectively excluded, i.e., the emission lines in each of the RIXS spectra are provided by the decay from one sole unoccupied orbital. Under the condition of narrow excitation it is evident that for a molecule with such a high symmetry as C_{60} the resonant (RIXS) spectra are much more sparse than the nonresonant spectrum. This fact reflects the strict parity and symmetry-selection rules operating for the RIXS transitions. The first selection for the RIXS transitions is dictated by the fact that the occupied orbitals should have the same parity as the unoccupied orbitals; e.g., RIXS, from the unoccupied orbital of ungerade (gerade) symmetry, displays only occupied orbitals of ungerade (gerade) symmetry. Further symmetry selection is given by the fact that the symmetries of allowed occupied orbitals for the RIXS transition should have symmetries Γ^0 and $\Gamma^0 \times h_g$, where the symbol Γ^0 represents the symmetry of the unoccupied orbital involved in the RIXS transition. For instance, for an unoccupied orbital with symmetry a_g, only occupied orbitals with symmetries a_g and h_g are

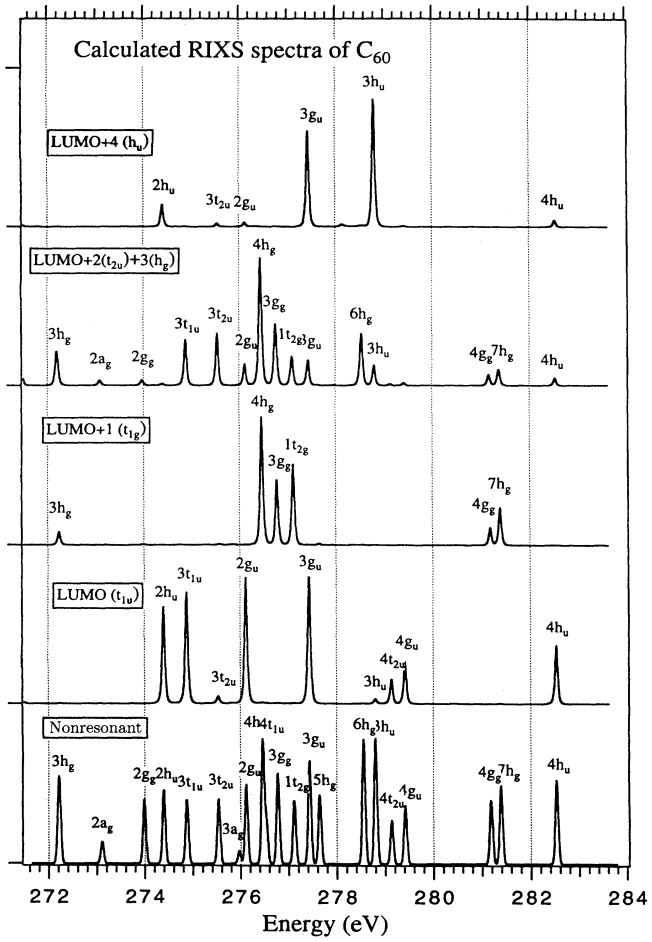

FIG. 5. Calculated nonresonant and resonant x-ray emission spectra. The lifetime of core-excited states is $\Gamma = 0.15$ eV, and the linewidth of incoming photons is $\gamma = 0.05$ eV.

allowed, while orbitals with t_{1g}, t_{2g}, or g_g symmetries are forbidden. For unoccupied orbitals with symmetries t_{1g}, t_{2g}, or g_g, occupied orbitals with a_g symmetry are forbidden. If the unoccupied orbital has h_g symmetry, no occupied orbitals with same parity as the unoccupied orbital are forbidden.

The relative emission intensities for different occupied orbitals in the RIXS spectra are evidently not the same as in the nonresonant, normal, x-ray emission spectrum, as shown in Fig. 5. This could be easily understood by considering the different mechanisms behind the nonresonant and resonant x-ray processes.

2. *Polarization and angular dependence for randomly oriented molecules*

When the core orbitals are near degenerate, as is the case for C_{60}, one needs in principle information from measurements using both linearly and circularly polarized excitations, for an unequivocal symmetry determination of occupied MOs when the symmetries of the unoccupied MOs are known (or vice versa). In Ref. 10, it was shown that the symmetries of the occupied MOs for molecules belonging to any of the 32 crystallographic point groups or to the two groups of linear molecules can be determined by measuring the so-called polarization ratios $P1$, $P2$, and $P3$, as defined in Eq. (28). In particular, it is possible to use the polarization ratios to determine the symmetries of the occupied orbitals of the C_{60} molecule belonging to the point group I_h. The instructions for this are collected in Table I.

The experimental spectra in this work are obtained with linear polarization, and therefore we investigate here the effect of different linear polarization directions. In this case the intensity expression for the polarization or angular dependences of the RIXS transitions has a quite simple form: If the linear polarization vectors of absorbed and emitted photons have an angle θ, the polarization dependence of the intensity of the emitted photons, $I(\theta)\propto\langle\sigma(\omega',\omega_0)\rangle$, can be expressed with help of Eqs. (24) and (25) as[29]

$$I(\theta)=I_0[1+R(3\cos^2\theta-1)] \tag{32}$$

and

$$R=\frac{1}{5}\left[\frac{3\sum_{\nu n}(\lambda^F_{\nu n}+\lambda^H_{\nu n})\Phi(\omega'+\omega_{\nu n}-\omega_0)}{2\sum_{\nu n}\lambda^G_{\nu n}\Phi(\omega'+\omega_{\nu n}-\omega_0)}-1\right], \tag{33}$$

where I_0 is proportional to the total intensity emitted in all directions and summed over all polarization vectors, and R is the polarization anisotropy. It should be noted that the classical formula for the polarization anisotropy parameter is valid only when one scattering channel ($k\rightarrow\nu, n\rightarrow k$) predominates:

$$R^{\text{class}}=\tfrac{1}{5}(3\cos^2\varphi-1), \tag{34}$$

where $\varphi\equiv\varphi^{kk}_{\nu n}$ is the angle between the dipole moments in the absorption and emission transitions, $\mathbf{d}_{\nu k}$ and $\mathbf{d}_{kn}$. This is the reason that, in contrast to the case of C_{60}, the polarization dependency of Cl K x-ray fluorescence of the CF_3Cl molecule[29] could be explained by this classic formula.

When the absorbed photon is linearly polarized, but emission photons unpolarized, $\cos^2\theta$ should be replaced by $\frac{1}{2}\sin^2\chi$ in Eqs. (32) or (25). χ is the angle between the polarization vector of the absorbed photon $\mathbf{e}_1$ and the propagation direction $\mathbf{k}_2$ of emission photon. Figure 6(a) illustrates RIXS spectra for $\theta=90°$ (dashed line) and $\theta=0°$ (solid line), respectively, when the linewidth of the incoming photon is 0.2 eV. In Fig. 6(b), the RIXS spectra for $\chi=90°$ (solid line) and $\chi=0°$ (dashed line) are shown. The angular dependence is found to be similar to the polarization dependence of case 1, but smaller. The comparison with the corresponding experimental measurements will be discussed in Sec. IV C 3.

3. *Tail excitation*

The shape of the RIXS signal is the result of the matching between the shape of the spectral function describing the incoming excitation and the lifetime widths and distributions of levels and sublevels in the core-excitation spectrum, as described by the total cross-section formulas given in Sec. IV C 2. This matching leads to different observable phenomena. We focus here on tail excitation, which we describe as the case when the bandpass covers more than one level or sublevel. We distinguish this from the Stokes shift and doubling, which involve only one resonance level.

i. Broadband excitation. Figure 7(a) and 7(b) illustrate the strong correlation between the spectral shapes of the absorbed and emitted photons. These figures show RIXS spectra of C_{60} when the linewidth of incoming photons has been assumed to be 0.2 or 1.0 eV, respectively. When the linewidth of the incoming photons is 0.2 eV, the RIXS spectra are by large the same as the narrow-band excitation spectra in Fig. 5. However, some small struc-

TABLE I. Use of polarization ratios for symmetry assignments of occupied MOs for the C_{60} molecule. x denotes an arbitrary value.

$P1$	$P2$	$P3$	$a_{g(u)}$	$t_{1g(u)}$	$t_{2g(u)}$	$g_{u(u)}$	$h_{g(u)}$	← unoccupied MO
x	x	x	$a_{g(u)}$	$t_{1g(u)}$	$t_{2g(u)}$	$g_{g(u)}$	$h_{g(u)}$	
x	$\frac{3}{2}$	x		$h_{g(u)}$	$h_{g(u)}$	$h_{g(u)}$	$g_{g(u)}$	
					$g_{g(u)}$	$t_{2g(u)}$	$t_{1g(u)}$	← occupied MOs
							$t_{2g(u)}$	
$\frac{3}{4}$	$\frac{3}{2}$	2	$h_{g(u)}$	$g_{g(u)}$	$t_{1g(u)}$	$t_{1g(u)}$	$a_{g(u)}$	
				$t_{2g(u)}$				

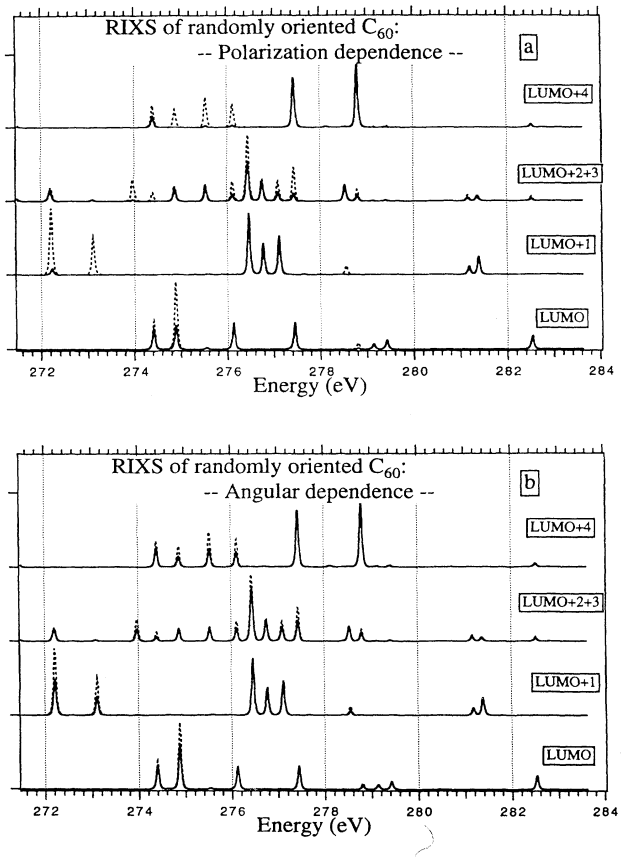

FIG. 6. Calculated polarization and angular dependence of RIXS spectra for randomly oriented C_{60} molecules.

tures appear as an effect of tail excitation from the nearby unoccupied orbitals. For broad linewidths of the incoming photons, tail excitation becomes progressively more important and could produce a considerable alteration of the appearance of the RIXS spectra. This is shown in the 1.0-eV excitation spectra of Fig. 7(b).

ii. Role of vibrational excitations. In electronic spectra generally only symmetric vibrational excitations receive significant intensities because only these shift the equilibrium point with accompanying large Franck-Condon factors. The vibrational levels of the core-excited states should therefore have the same symmetries as the corresponding pure electronic states, and the vibrational excitations in absorption or emission should therefore to a first approximation not change the symmetry-related intensity features in the RIXS spectra, and, in particular, the polarization properties and angular dependences of RIXS should remain the same. The role of vibrational excitations becomes important rather through the effect of tail excitation. In the preceding the core-excited energies were taken as the experimental values which correspond to the band maxima, i.e., the vertical energies. The width of the core-excited states indicates that these maxima correspond to highly excited vibrational levels. A simulation has been made to take account of the vibrational excitations following core absorption. We first assume that all these states have the same vibrational structures, that the maximum of the absorption peak corresponds to the vibrational state $v=m$, and consider a series of states from $v=0$ to $v=2m$ with splittings of 0.2 eV. Figure 7(c) shows a RIXS spectrum corresponding to the case when the vibronic intensities in the x-ray absorption follow a Lorentzian distribution with a linewidth of

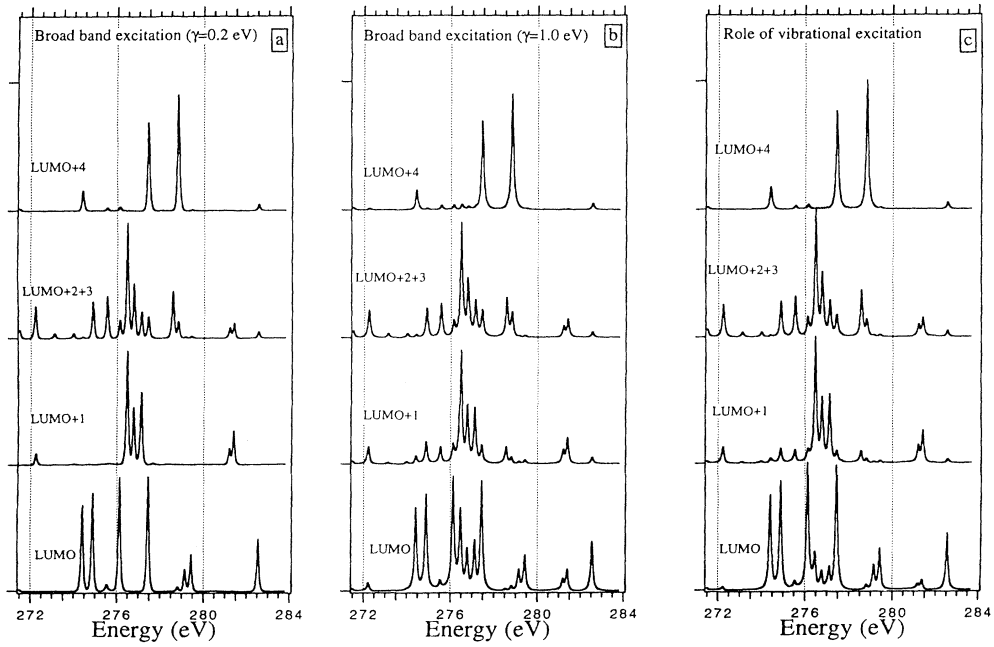

FIG. 7. The calculated RIXS spectra with different linewidths for incoming photons. (a) $\gamma=0.2$ eV. (b) $\gamma=1.0$ eV. (c) Simulating the role of vibrational tail excitation, $\gamma=0.2$ eV and $2\Gamma=0.15$ eV.

0.5 eV and with a maximum at $m=5$. The linewidth of the incoming photons is 0.2 eV, which is the same as that for Fig. 7(a). The difference between Figs. 7(c) and 7(a) can be understood by that vibrational excitations have made the tail excitation more effective. Actually, the spectra shown in Fig. 7(c) are similar to the ones excited by broadband incoming photons (1.0 eV), shown in Fig. 7(b). On the other hand, using a Gaussian distribution of the vibronic intensities with the same parameters, the tail excitation is much decreased and Fig. 7(c) will in that case be more similar to Fig. 7(a), i.e., to the narrow-band excitation case.

iii. Vibronic coupling and Jahn-Teller distortions. The RIXS transitions are strictly controlled by the symmetry selection, which creates sparse electronic RIXS spectra of C_{60} in the limit of narrow-band excitation; see Sec. IV C 1. It is well known in many other electronic spectroscopies that vibronic coupling may introduce transitions that are electronically forbidden. This is manifested in, for instance, two-photon spectroscopy,[42,43] which is closely related to RIXS. The possible vibronic modes which can produce symmetry-allowed transitions via vibronic coupling are governed by the fact that the product of irreducible representations $\Gamma_\nu \times \Gamma_\alpha \times \Gamma_\beta \times \Gamma_n$, where ν and n denote unoccupied and occupied orbitals and α and β dipole moment components, must contain the totally symmetric representation. Vibronic coupling may operate among the initial and final orbitals of RIXS transitions. For a molecule as large as C_{60}, there are many vibrational modes with different symmetries which might introduce electronically disallowed transitions through vibronic coupling. The frequencies of vibronic modes in neutral C_{60} range up to 0.2 eV.[44] For C_{60} one can expect severe Jahn-Teller distortions due to the extreme high degeneracy. For instance, the lowest core-excited states, such as those excited from core orbitals h_g to LUMO t_{1u}, could couple with the normal modes of g parity $([t_{1u}\times t_{1u}]=a_g+h_g;\quad [h_g\times h_g]=a_g+t_{1g}+t_{2g}+2g_g+2h_g)$. It has been predicted theoretically for the lowest singlet state of C_{60} that Jahn-Teller distortion plays the most crucial role for modes with frequencies within 0.1 eV.[45] Similar features can be expected for Jahn-Teller distortions of core-excited states.

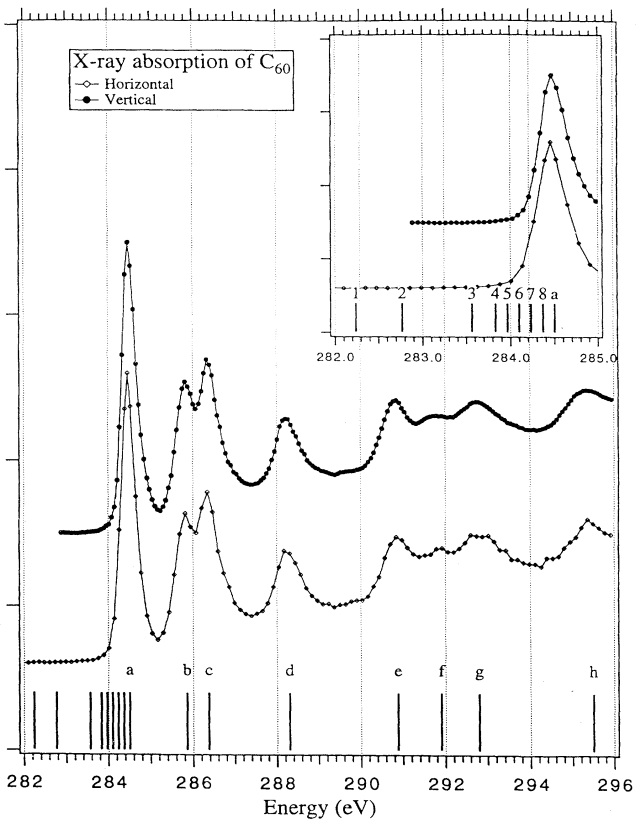

FIG. 8. X-ray-absorption spectra of C_{60} near the C K edge, obtained with total-electron-yield detection at the horizontal and vertical positions. The bars indicate the resonant excitation energies.

Unfortunately, calculations of the effect of vibronic coupling are still too complex to carry out for C_{60}. However, by considering vibronic coupling one can expect the RIXS spectrum for the LUMO level to be quite different from the one shown in Fig. 7(a) when the linewidth of the incoming photons is 0.2 eV. Rather it would look like the 1.0-eV excitation spectrum shown in Fig. 7(b), due to the excitation of nearby vibronic modes with different parities. The effect of tail excitation can effectively be excluded either by narrowing the linewidth of the incoming photons, or by tuning their energies as far as possible from the nearby resonance. An experimental example for the latter case is given by the band-gap-excited spectra discussed in Sec. V A. Using this method, the RIXS spectrum is purified in the sense that tail excitation vanishes, and it becomes the product of symmetry-selection rules applied to the LUMO zero-level only.

V. COMPARISON WITH EXPERIMENT

A. Band-gap excitations

As shown in the previous sections, the determination of energies for the core-excited states is very important for describing the RIXS process. The two x-ray absorption spectra of C_{60}, shown in Fig. 8, were taken in the total electron yield mode at the two different geometries used to record emission parallel and perpendicular, respectively, to the exciting photon polarization. As expected the spectra are almost identical, and in good agreement with other results.[4–6] The assignments of the spectra were discussed in Sec. IV B 2. The bars in Fig. 8 indicate the excitation energies at which the x-ray emission spectra were recorded.

In Fig. 9 we present a series of Stokes-shifted spectra recorded at different excitation energies. The latter are indicated in the x-ray absorption spectrum shown in Fig. 8 from $1-a$. The last detuning energy is as low as 282.2 eV, 2.3 eV below the upper band-gap edge defined by the LUMO level. In addition to the inelastic part Fig. 9 also indicates Stokes features in the elastic (REXS) part of the spectra. As we mentioned in Sec. IV C 3, the tail excitation could be removed from those measurements. By considering the linewidth of incoming photons in this experiment, the effect of tail excitation is only possible from

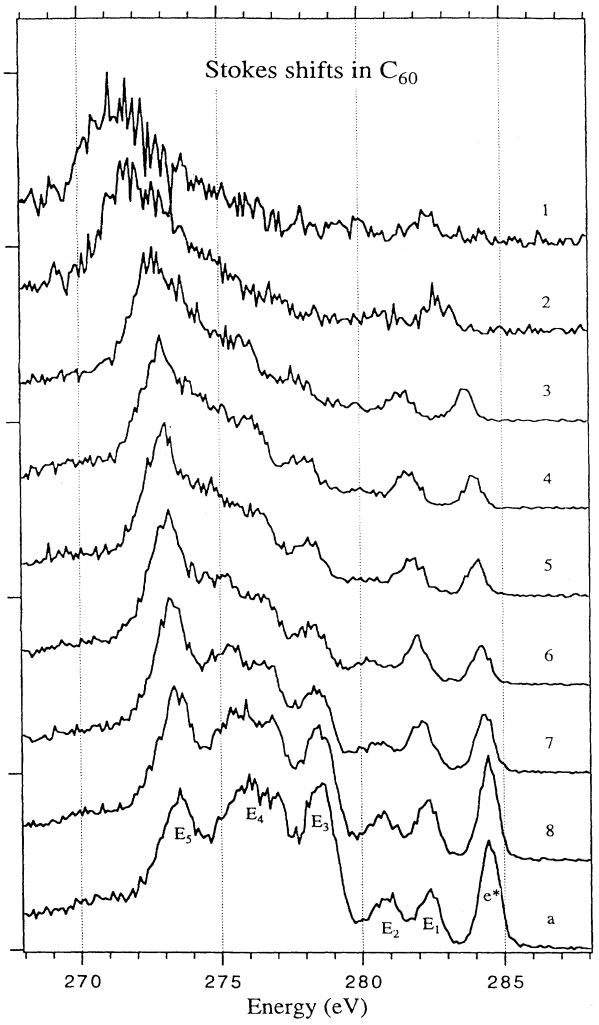

FIG. 9. Stokes shifted RIXS spectra of C_{60} obtained at the excitation energies marked in Fig. 8.

the vibronic coupling.

The RIXS spectra also show, apart from detuning energy shifts, broadening and relative enhancements of the low-energy features. These enhanced features derive mostly from the E_5 structure in the LUMO resonance spectrum. The depletion of the intermediate and high-energy regions of the RIXS spectra as one proceeds through larger detuning energies is an important consequence of band-gap excitation. Features E_2, E_3, and E_4 are present for the excitation of 284.5 eV, close to the LUMO resonance, while they are depleted at 282.3 eV. From a symmetry analysis the E_2 feature is a forbidden LUMO-RIXS transition, and significant parts of E_3 and E_4 as well (for instance, the $6h_g$ contribution in E_3). Their presence at 284.5 eV is to a large extent an effect of tail excitation from vibronic coupling modes with g parity. Actually, the role of vibronic coupling is indicated by comparing the RIXS spectra generated at the vertical band-maximum position of the LUMO band (excitation point a at 284.5 eV) with the spectrum generated close to the adiabatic point (excitation point 6 at 284.1 eV). Despite the small energy difference of 0.4 eV the two spectra are quite different; the latter is symmetry purified while the former is composite. We interpret this observation as meaning that the spectrum generated at the adiabatic point is dominated by the zero vibrational level which has the pure electronic symmetry, here t_{1u}, leading to a clean RIXS spectrum, while the spectrum generated at the vertical point is a composite of the vibronically induced nonsymmetric modes, thus resulting from internal tail excitations involving many symmetries.

While the E_5 feature is enhanced in accordance with parity and, in particular, symmetry-selection rules as applied to RIXS originating from the LUMO level, we thus observe that the symmetry-forbidden transitions are depleted as the RIXS spectra become determined from one sole resonance level only, here the t_{1u} zero LUMO level. We can therefore interpret the Stokes features presented in Fig. 9 as due to a strict enforcement of the symmetry selection rules for the high isocahedral point group of C_{60}. In particular, parity selection sustains the *symmetry-restricted* interpretation of molecular RIXS, and the notion of delocalized core electron excitation. These observations, and the change of spectral shape, are backed by the simulations presented in Fig. 10.

Apart from a purification in the Stokes region due to symmetry selection, the spectra become shifted and distorted due to a delicate dependence on core-hole state lifetime, on detuning frequency (as is obvious from Fig. 9), and the shape of the excitation spectral function. We have simulated the dependence of these parameters; the results are shown in Fig. 10. Out of these parameters the frequency and band pass [full width at half maximum (FWHM)] are well determined experimentally (the FWHM of 0.2 eV has been used in the experimental spectra shown), while the shape of the excitation function and the lifetime are in general unknown parameters (a Gaussian function has been used in Fig. 10). The area restricting the observation of Stokes doubling is quite narrow for Gaussians, with a quite complex relation between Γ and Γ_Φ; see Sec. III B. For Stokes doubling in the Gaussian case the normal peak can easily be drowned by the Stokes peak, especially when there are other (here vibrational) degrees of freedom present. Other limiting cases for the spectral functions give quite different constraint areas for observation of Stokes doubling. In reality one may end up in combined functions, e.g., Voigt functions, or in tail-cut functions with complex analytical properties and consequences for the RIXS signal.

In the simulated spectra of Fig. 10, we have for simplicity assumed a pure t_{1u} character of the resonant LUMO level, without vibrational broadening and tail contributions from the vibronic modes. This restriction gives a good representation of all Stokes-shifted spectra, but a rather poor resonant LUMO spectrum (position a), due to a lack of contributions from vibronically induced transitions as mentioned above. The E_1 and E_5 features are due to contributions from valence orbitals with u parity, as indicated in Fig. 5. Those two features are well described by the simulated spectra for all cases. This indi-

cates that the vibronically induced transitions appearing in the resonant LUMO spectrum (position *a*) derive from the modes with gerade (*g*) parity. However, it is understandable that when the excitation energy is very deep in the gap, the relative strength of tail excitations from nearby vibronic levels becomes larger. This may partly be responsible for the enhancements of feature E_5 at positions 1 and 2 in Fig. 10.

For Gaussian functions one obtains experimental concordance for realistic Γ values. The dependence of the Stokes-shifted spectra on the lifetime is not so strong for Gaussian functions as it would be for, e.g., Lorentzian functions (from simulations of the same type as those giving Fig. 10, we can discard, Lorentzian functions as unrealistic). The simulations with Gaussian functions indicate that the lifetime of the core-excited LUMO level should be confined to the interval 0.05–0.3 eV for C_{60}. This is what can be expected from measurements of smaller carbon-containing molecules [e.g., $2\Gamma=0.15$ eV for the C 1*s* π^* level of CO_2 (Ref. 46)].

B. Resonant excitations

The RIXS spectra of C_{60}, excited at various photon energies indicated by *a*–*h* in Fig. 8, with the detector placed at the vertical position perpendicular to the exciting polarization, are displayed in Fig. 11. The spectral profile shows a strong dependence on the excitation energies below the ionization threshold. Well below the ionization threshold, the density of core-excited states is small, and the excitation frequencies can be tuned to be selectively resonant with individual or a few individual states of certain symmetries. The strong symmetry selection in the RIXS process is indeed demonstrated by Fig. 11. For higher energies involving a higher density of core-excited states, the RIXS spectra become similar to the broadband-excited or the nonresonant spectra. The pronounced features in the RIXS spectra shown in Fig. 11 are labeled E_1, E_2, E_3, E_4, and E_5. It can be seen that when the photon energy is shifted from 284.5 to 285.85 eV, the intensity of E_1 becomes stronger relative to E_2 and E_3. The relative intensity of E_1 increases at a photon energy of 286.37 eV and decreases at a photon energy of 288.3 eV. The E_4 feature has a different behavior from the E_1, E_2, and E_3 features. It changes only slightly with frequency, probably because it contains quite many close-lying states with different symmetries. The E_5 feature is clearly resolved at the photon energy of 284.5 eV, but appears only as a shoulder at other photon energies.

A comparison between the experimental and simulated spectra at photon energies of 284.5, 285.85, 286.37, and 288.3 eV is shown in Fig. 12. The simulated spectra are based on the calculated spectra shown in Fig. 7(a) convoluted by an experimental broadening of 0.4 eV. These are "pure" electronic contributions, excluding tail excitation from vibronically induced transitions. Such a comparison could be used to identify the vibronic contribution to the experimental RIXS spectra, which was discussed in Sec. V A for the spectrum referring to the LUMO orbital. It is clearly indicated that the vibronically induced transitions have significant contributions. However,the main trends of the spectral profiles going from low to high excitation frequencies, scanning LUMO through LUMO+4 orbitals, are still reasonably described by the pure electronic simulations. The spectra at photon energies of 285.8 and 286.4 eV are quite similar, which reflects the fact that LUMO+1 and (LUMO+2, LUMO+3) are closely located in energy.

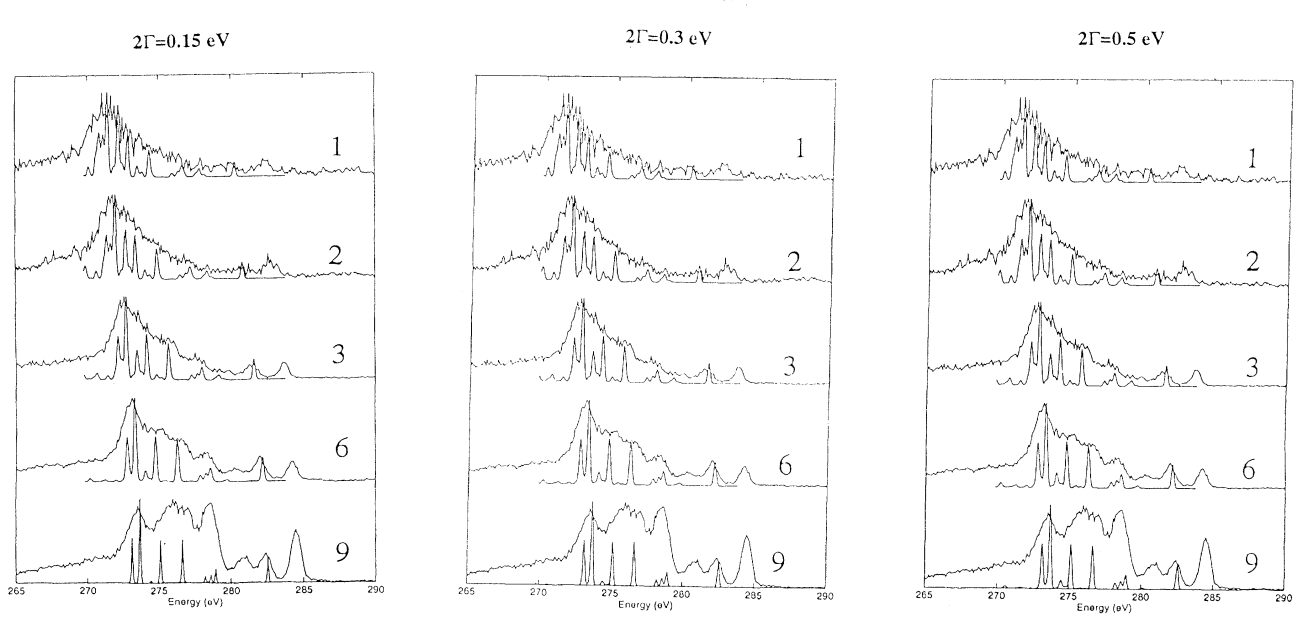

FIG. 10. Experimental and simulated Stokes-shifted RIXS spectra for different lifetimes. Gaussian excitation functions of FWHM 0.2 eV are used. (Note that "9" refers to "*a*" in Fig. 8.)

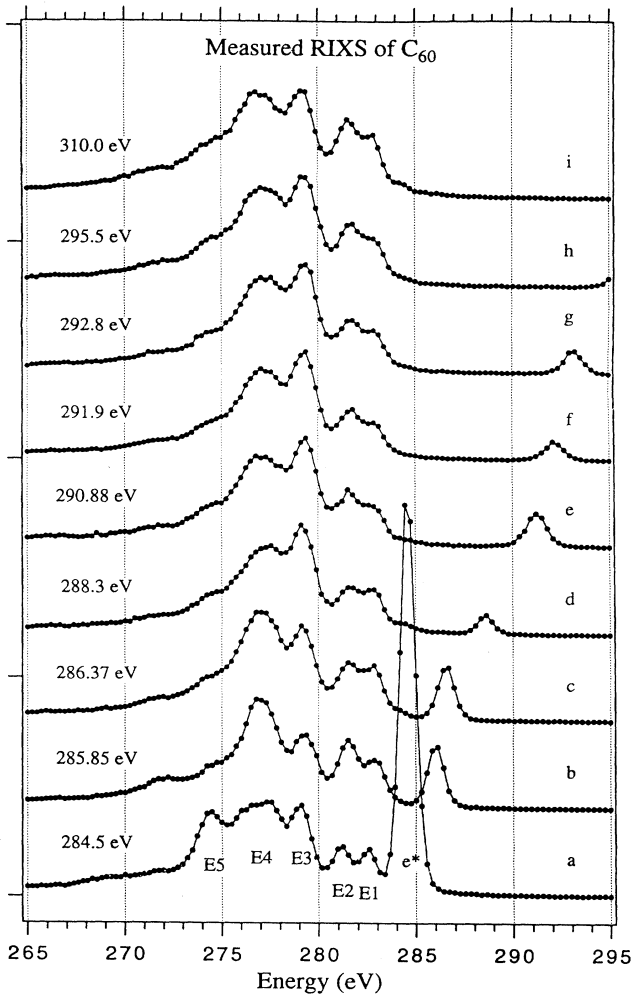

FIG. 11. RIXS spectra of C_{60} obtained with various photon excitation energies, recorded at the vertical position.

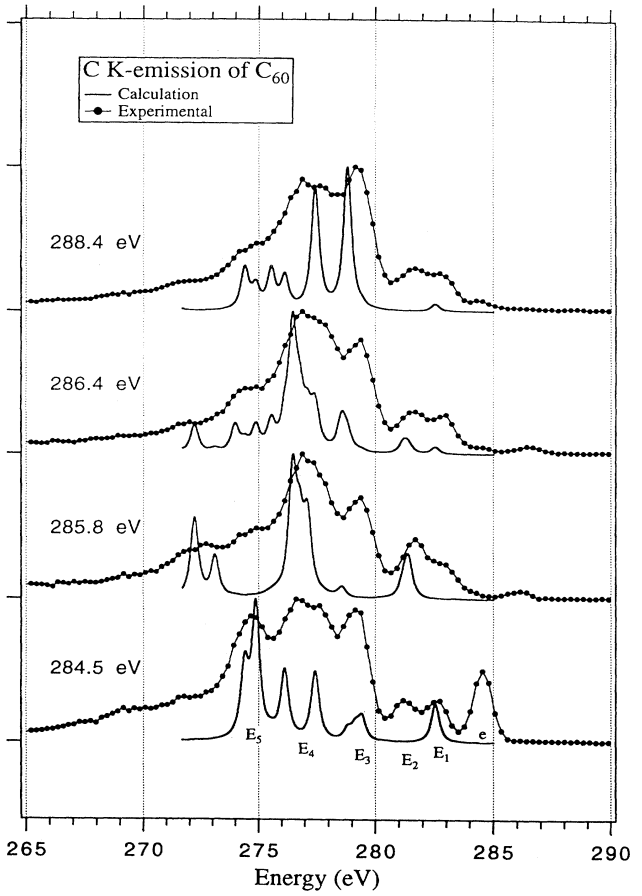

FIG. 12. The experimental and calculated RIXS spectra of C_{60} below the ionization threshold.

As discussed in connection with the nonresonant spectrum in Sec. IV A the spectral features are of different complexity with respect to a MO analysis. Thus while the highest occupied molecular orbital (HOMO) and HOMO-1 are quite simple (assigned as $4h_u$ and $4g_g+7h_g$, respectively), the E_4 structure contains not less than six near-degenerate MO's ($5h_g+3g_u+3g_g+4t_{1u}+4h_g+2g_u$). Of particular interest is the fact that E_5 is dominated by ungerade contributions ($3t_{1u}+2h_u$ in addition to $2g_g$), and that it correlates strongly with excitation to the LUMO level ($5t_{1u}$). We see this as a confirmation of the parity-selection rule associated with RIXS spectra.[22] The REXS peak (peak e) is very strong when the exciting photon beam is tuned to the first LUMO level. At higher resonant excitation energies this elastic peak is considerably weaker. As expected, the elastic peak becomes more dominating for vertical (perpendicular) emission than for emission in the horizontal plane (parallel to the polarization of the exciting photons). Ignoring polarization effects the relative intensities of these REXS transitions should relate quadratically with respect to the corresponding absorption peaks (they involve four rather than two identical transitions moments) which is not far from being the case, cf. Figs. 8(a) and 11. Properties of REXS spectra differ from the corresponding RIXS spectra in several aspects, in particular concerning lifetime interference and polarization effects, and we postpone the analysis of the REXS spectra of C_{60} to a later date.

Figure 13 shows the angular dependence of soft-x-ray fluorescence spectra of C_{60} obtained by recordings at both horizontal and vertical emission directions. This corresponds to the third case discussed in Sec. IV C 2. The x-ray fluorescence was normalized such that the integral intensity of the low-energy flank region between 268 and 273 eV is the same for the horizontal and vertical detection positions. With this normalization it is noted that the x-ray fluorescence profiles recorded at the vertical position are lifted for all prominent RIXS features at excitation energies below the ionization threshold. At a photon excitation energy of 310 eV the profiles of the x-ray fluorescence are identical for the two detected positions. The vibronically induced transitions have a significant influence on the RIXS spectra, as shown in Fig. 12. It was discussed in Sec. IV C 3 that such vibronic contributions can somehow be simulated by broadband excitation. The calculated spectra shown in Fig. 13 are thus obtained

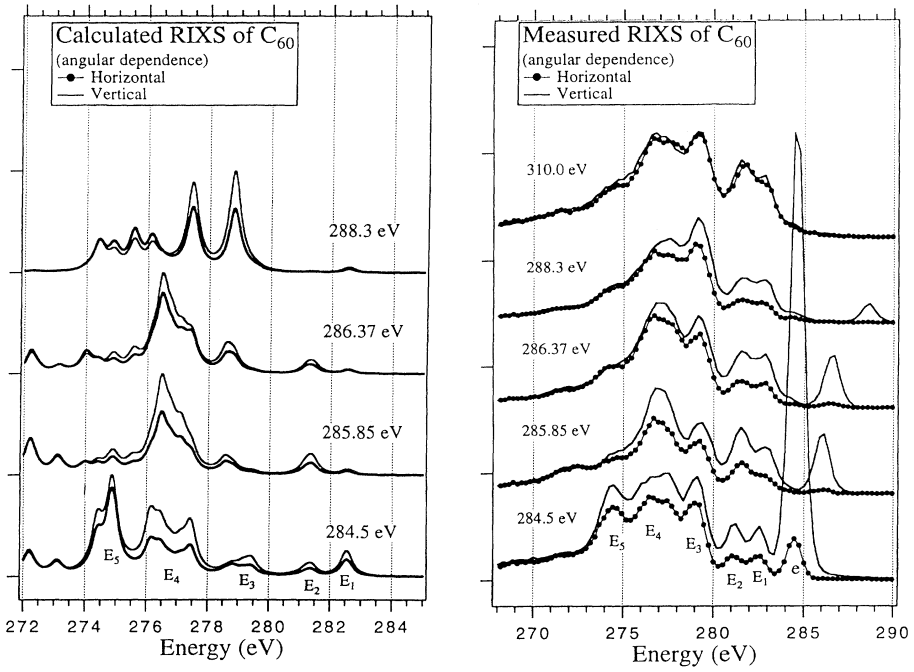

FIG. 13. The angular dependence of RIXS spectra of C_{60}. The experimental (left) and calculated (right) RIXS spectra are obtained at the horizontal and vertical positions.

with the same conditions as that for Fig. 7(b), i.e., a linewidth of 1.0 eV is used for the incoming photons. A comparison with simulations is aggravated by the somewhat arbitrary choice of normalization to be made in both the experimental and theoretical spectra. Normalizing the two profiles at the low-energy flank in the simulated cases, we obtain an angular dependence that is in quite good accordance with the experimental one for the intensive group of features comprising E_3, E_4, and E_5, but which underestimates the larger angular effects for the weaker E_1 and E_2 bands, although the correct trends are obtained even for these. Some of this deviation can probably be due to the incoherent contributions not fully included in the simulation, but perhaps also to polarization discriminations in the soft-x-ray detector used in the experiment. It can be seen that the overall angular dependence is not very strong, something that can be understood by the high degree of degeneracy of MOs in C_{60}.

VI. SUMMARY

Using C_{60} as a far-reaching molecular test case, we have shown in this work that resonant inelastic x-ray scattering spectroscopy (RIXS) provides a potentially rich method for electronic structure investigations. We have validated the use of Kramers-Heisenberg resonant scattering theory for describing RIXS, and extracted its consequences for symmetry- and polarization-selective scattering spectra according to a formulation recently given in Refs. 10 and 22, and which was further elaborated here. Many effects or processes contributing to the total RIXS cross section can be derived from this common formulation, and their isolated behaviors have here been simulated with C_{60} as a framework and using *ab initio* computational data as the building blocks.

It has become obvious that symmetry selection leads to a strong frequency dependence of the RIXS signal, and that the shapes of the RIXS spectra are strongly correlated to shapes of the spectral functions describing the incoming excitation photons. The strong symmetry selection, including the parity-selection rule, is here verified by the RIXS spectra of C_{60}. For a molecule with a high symmetry the RIXS spectra pertaining to the lower well-separated resonance levels become very sparse in the limit of narrow excitation band passes. In addition to the symmetry selectivity, the matching between the shape of the spectral function describing the incoming excitation and the shape and distribution of levels and sublevels in the core-excitation spectrum is an important factor for the strong frequency dependence of RIXS spectra. This matching leads to effects like the tail excitation and Stokes shifts (Stokes doubling) described in some detail in this work. Tail excitation is the primary reason that RIXS spectra grow complex and appear similar to the corresponding nonresonant spectra for the dense resonances at higher core-excitation energies and for broader excitation bandpasses. The tail excitation is much enhanced by the vibrational progressions accompanying core excitation, and by the presence of vibronic coupling. Its strength was directly proven here by showing that a few structures, which by symmetry cannot derive the first LUMO level, strongly varied with respect to the symmetry-allowed structures when the excitation energy spanned the low-energy flank of the first core-absorption band.

The one-step formalism differs distinctly from the conventional two-step models used in several previous works for x-ray fluorescence spectra. The differences between one- and two-step models are apparent already in the unpolarized case, but become even more conspicuous for the polarization anisotropy. We find that Stokes doubling is apparent under special conditions. The condi-

tions differ significantly for the limiting cases of the photon spectral functions, being quite restricted for Gaussian functions. This illustrates the fact that the experimental determination of the excitation spectral functions becomes a prerequisite for conducting an accurate analysis of the RIXS spectra, and that narrowing of the excitation functions without the control of, for instance, their flanks, may even destroy the informational content of the generated RIXS spectra. The C_{60} molecule with its high isocahedral symmetry illustrates that Stokes-shifted spectra have particular consequences for symmetry selection of RIXS. Most conspicuous are the spectra following band-gap excitation. These become symmetry purified, but also strongly distorted because of the delicate dependence on both frequency and form of the spectral functions for the excitation photons. The agreement between the simulations and the band-gap-excited spectra proves the selectivity based on the full, nonbroken, point-group symmetry, and that the RIXS spectra can be understood by assuming delocalized core electrons and delocalized core-hole states. The sharpening or broadening of the Stokes lines can also be used to determine lifetimes, and presumably also, for simpler systems than investigated here, vibrational and geometrical properties of the molecule.

Other important RIXS features are the polarization and angular dependences, explored here for randomly oriented or ordered C_{60} molecules. Other relevant aspects are discussed qualitatively in the present work, namely state-lifetime interference effects, the influence of vibronic coupling, and the core-hole localization problem. In analogy with general two-photon spectroscopy, it is argued that vibronic coupling is an important incoherent factor in RIXS, which may destroy some of the selective character based on electronic symmetry rules only. Numerical demonstrations of the importance of vibronic coupling and other RIXS effects for a set of selected small molecules are now in progress.

ACKNOWLEDGMENTS

Olav Vahtras is acknowledged for having performed *ab initio* calculations on C_{60} on which much of the present analysis is based. This work was supported by CRAY Research Inc. and the Swedish Natural Science Research Council (NFR), and the Göran Gustafssons Foundation for Research in Natural Science and Medicine. We would like to thank T. Warwick, P. Heimann, E. Rotenberg, and J. D. Denlinger for assistance during the measurements. The work at ALS, Lawrence Berkeley Laboratory, was supported by the director, Office of Energy Research, Office of Basic Energy Science, Material Sciences Division of the U.S. Department of Energy, under Contract No. DE-AC03-76SF00098.

[1]J. H. Weaver, J. L. Martins, T. Komeda, Y. Chen, T. R. Ohno, G. H. Kroll, N. Troullier, R. E. Haufler, and R. E. Smalley, Phys. Rev. Lett. **66**, 1741 (1980).

[2]P. A. Brühwiler, A. J. Maxwell, A. Nilsson, R. L. Whetten, and N. Mårtensson, Phys. Lett. **193**, 311 (1992).

[3]G. Gensterblum, J. J. Pireaux, P. A. Thiry, R. Caudano, J. P. Vigneron, P. Lambin, A. Lucas, and W. Krätschmer, Phys. Rev. Lett. **67**, 2171 (1991).

[4]E. Sohmen, J. Fink, and W. Krätschmer, Europhys. Lett. **17**, 51 (1992).

[5]C. T. Chen, L. H. Tjeng, P. Rudolf, G. Meigs, J. E. Rowe, J. Chen, J. P. McCauley, Jr., A. B. Smith III, A. R. McGhie, W. J. Romanow, and E. W. Plummer, Nature **352**, 603 (1991).

[6]L. J. Terminello, D. K. Shuh, F. J. Himpsel, D. A. Lapiono-Smith, J. Stöhr, D. S. Bethune, and G. Meijer, Chem. Phys. Lett. **182**, 491 (1991).

[7]B. Wästberg, S. Lunell, C. Enkvist, P. A. Brühwiler, A. J. Maxwell, and N. Mårtensson, Phys. Rev. B **50**, 13 031 (1994).

[8]P. A. Brühwiler, A. J. Maxwell, P. Rudolf, C. D. Gutleben, B. Wästberg, and N. Mårtensson, Phys. Lett. **193**, 311 (1992).

[9]J. H. Guo, Y. Luo, O. Vahtras, P. Skytt, N. Wassdahl, H. Ågren, and J. Nordgren, Chem. Phys. Lett. **227**, 98 (1994).

[10]Y. Luo, H. Ågren, and F. K. Gelmukhanov, J. Phys. B **27**, 4169 (1994).

[11]F. Kh. Gel'mukhanov, L. N. Mazalov, A. V. Nikolaev, A. V. Kondratenko, V. G. Smirnii, P. I. Wadash, and A. P. Sadovskii, Dok. Akad. Nauk SSSR **225**, 597 (1975).

[12]F. Kh. Gel'mukhanov, L. N. Mazalov, and N. A. Shklyaeva, Zh. Eksp. Teor. Fiz. **69**, 1971 (1975) [Sov. Phys. JETP **42**, 1001 (1975)].

[13]F. Kh. Gel'mukhanov, L. N. Mazalov, and N. A. Shklyaeva, Zh. Eksp. Teor. Fiz. **71**, 1960 (1976) [Sov. Phys. JETP **44**, 504 (1976)].

[14]F. Kh. Gel'mukhanov, L. N. Mazalov, and A. V. Kondratenko, Chem. Phys. Lett. **46**, 133 (1977).

[15]F. Kh. Gel'mukhanov and H. Ågren, Phys. Rev. A **50**, 1129 (1994).

[16]T. Åberg, Phys. Scr. **21**, 495 (1980).

[17]T. Åberg and G. Howat, in *Theory of the Auger Effect,* edited by S. Flügge and W. Melhorn, Handbuch der Physik Vol. 1 (Springer, Berlin, 1982).

[18]T. Åberg and J. Tulkki, in *Atomic Inner Shell Physics,* edited by B. Crasemann (Plenum, New York, 1985).

[19]T. Åberg and B. Crasemann, in *X-ray Resonant Scattering,* edited by G. Materlik, K. Fischer, and C. Sparks (Elsevier, New York, 1993).

[20]Y. Ma, N. Wassdahl, P. Skytt, J. H. Guo, J. Nordgren, P. D. Johnson, J. E. Rubensson, T. Boske, W. Eberhardt, and S. Kevan, Phys. Rev. Lett. **69**, 2598 (1992).

[21]Y. Ma, Phys. Rev. B **49**, 5799 (1994).

[22]F. Kh. Gel'mukhanov and H. Ågren, Phys. Rev. A **49** (1994).

[23]T. Warwick, P. Heineman, D. Mossessian, and H. Padmore, Rev. Sci. Instrum. **66**, 2037 (1995).

[24]J. Nordgren and R. Nyholm, Nucl. Instrum. Methods Phys. Res. Sect. A **246**, 242 (1986).

[25]J. Nordgren, G. Bray, S. Cramm, R. Nyholm, J. E. Rubensson, and N. Wassdahl, Rev. Sci. Instrum. **60**, 1690 (1989).

[26]J. J. Sakurai, in *Advanced Quantum Mechanics,* edited by M. Hamermesh (Addison-Wesley, Reading, MA, 1967).

[27]W. M. McClain, J. Chem. Phys. **55**, 2789 (1971).

[28]D. W. Lindle, P. L. Cowan, R. E. LaVilla, T. Jach, R. D. Deslattes, B. Karlin, J. A. Sheehy, T. J. Gil, and P. W. Langhoff, Phys. Rev. Lett. **60**, 1010 (1988).

[29]S. H. Southworth, D. W. Lindle, R. Mayer, and P. L. Cowan,

Phys. Rev. Lett. **67**, 1098 (1991).
[30]F. Kh. Gel'mukhanov and H. Ågren, Phys. Lett. A **193**, 375 (1994).
[31]G. B. Armen and H. Wang, Phys. Rev. A **51**, 1241 (1995).
[32]The calculated nonresonant x-ray emission spectrum shown in Fig. 2 differs slightly from the one presented in the figure of Ref. 9, because the transition moments for orbitals of t_{2u} and t_{2g} symmetry were missing. However, the main conclusions presented here for the nonresonant spectrum are still the same as the ones of Ref. 9.
[33]B. Wästberg and A. Rosén, Phys. Scr. **44**, 276 (1991).
[34]R. Viruela-Martín, P. M. Viruela-Martín, and E. Ortí, J. Chem. Phys. **96**, 4474 (1992).
[35]S. Satpathy, Chem. Phys. Lett. **130**, 545 (1986).
[36]P. Glans, R. LaVilla, Y. Luo, H. Ågren, and J. Nordgren, J. Phys. B **27**, 3399 (1994).
[37]A. H. H. Chang, W. C. Erlemer, and R. M. Pitzer, J. Chem. Phys. **95**, 9288 (1991).
[38]R. Manne, J. Chem. Phys. **52**, 5733 (1970).
[39]E. Ortí and J. L. Brédas, J. Chem. Phys. **89**, 1009 (1988).
[40]E. Ortí and J. L. Brédas, Chem. Phys. Lett. **164**, 247 (1989).
[41]E. Ortí, M. C. Piqueras, R. Crespo, and J. L. Brédas, Chem. Mater. **2**, 110 (1990).
[42]Y. Luo, H. Ågren, S. Knuts, B. Minaev, and P. Jørgensen, Chem. Phys. Lett. **209**, 513 (1993).
[43]Y. Luo, H. Ågren, S. Knuts, and P. Jørgensen, Chem. Phys. Lett. **213**, 356 (1993).
[44]R. E. Stanton and M. D. Newton, J. Phys. Chem. **92**, 2141 (1987).
[45]S. Suzuki, D. Inomata, N. Sashide, and K. Nakao, Phys. Rev. B **48**, 14 615 (1993).
[46]M. Tronc, G. C. King, and H. Read, J. Phys. B **12**, 137 (1979).